1966-05

Electron paramagnetic resonance analysis of dimethyl amidogen in polycrystalline tetramethyl tetrazene.

Eikel, Harvey Andrew.

Monterey, California: U.S. Naval Postgraduate School

ELECTRON PARAMAGNETIC RESONANCE ANALYSIS OF DIMETHYL AMIDOGEN IN POLYCRYSTALLINE TETRAMETHYL TETRAZENE

HARVEY ANDREW EIKEL

ELECTRON PARAMAGNETIC RESONANCE ANALYSIS OF DIMETHYL AMIDOGEN IN POLYCRYSTALLINE TETRAMETHYL TETRAZENE

By

Harvey Andrew Eikel
Lieutenant, United States Navy
B.S., University of Texas, 1958

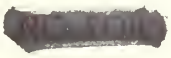

Submitted in partial fulfillment
for the degree of

MASTER OF SCIENCE OF CHEMISTRY

from the

UNITED STATES NAVAL POSTGRADUATE SCHOOL
May 1966

ABSTRACT

The photolytic decomposition of tetramethyl-2-tetrazene yields a short-lived paramagnetic species which is stabilized at liquid nitrogen temperatures. From the analysis of the electron paramagnetic resonance spectrum the species has been identified as the free radical dimethyl amidogen. The hyperfine coupling tensors were assigned on the basis of a polycrystalline line shape analysis. The radical exhibits axial symmetry with the parallel components of the tensors greater than the perpendicular components. The limits of error associated with the components of the tensors were estimated from the general comparison of the calculated and observed spectra. The principal values of the hyperfine coupling and g tensors for the radical are:

A^N isotropic $= 27.9 \pm 3.0$G. $A^N_{\parallel} = 27.9 \pm 3.0$G. $A^N_{\perp} = 27.9 \pm 3.0$G.

A^H isotropic $= 26.4 \pm 1.0$G. $A^H_{\parallel} = 28.4 \pm 1.0$G. $A^H_{\perp} = 25.5 \pm 1.0$G.

$g_{\parallel} = 2.0098 \pm 0.0015$ $g_{\perp} = 2.0042 \pm 0.0005$

TABLE OF CONTENTS

LIST OF ILLUSTRATIONS

LIST OF ILLUSTRATIONS (CONT'D)

LIST OF ILLUSTRATIONS (CONT'D)

1. Introduction

One may characterize the endeavors of this investigation in two rather broad but interrelated areas. The first of these is the attempt to produce a specific radical species in liquid-phase media and in condensed-phase media. The second area is the attempt to abstract data from each of the above spectra and thereby investigate the usefulness of an existing mathematical algorithm whereby radicals in the polycrystalline phase may be totally characterized.

Before defining total characterization, an examination of the spin Hamiltonian in general terms will be necessary. The effective spin Hamiltonian for the system in question can be written [31],[1]

$$\mathcal{H} = \beta_e \vec{S} \cdot \vec{\vec{g}} \cdot \vec{H} - \sum_i \beta_n g_{ni} \vec{I}_i \cdot \vec{H} + \sum_i \vec{S} \cdot \vec{\vec{A}}_i \cdot \vec{I}_i$$

where $\vec{H}$ is the steady applied magnetic field; $\vec{S}$ and $\vec{I}_i$ are the electron and nuclear spin operators; β_e and β_n are the Bohr electron and nuclear spin magnetrons; g_{ni} the nuclear spectroscopic splitting factor; $\vec{\vec{g}}$ the electron spectroscopic splitting tensor; and $\vec{\vec{A}}_i$ the hyperfine coupling tensors. The summation is taken over all the interacting nuclei in each term of the Hamiltonian.

In this Hamiltonian, the first expression is referred to as the electron Zeeman term, which arises from the interaction of the electron with the applied magnetic field. The second expression is the nuclear Zeeman term, which arises

from the interaction of the nucleus with the applied magnetic field. The last expression is the hyperfine term which arises from the interaction of the electron and the nucleus.

The anisotropy of the $\vec{g}$ tensor is related to the spin-orbit coupling, which introduces a contribution of the otherwise quenched orbital angular momentum to the electronic magnetic moment. The anisotropy of the hyperfine couplings may be interpreted as resulting from dipole-dipole interactions between the electron spin distribution and the magnetic nuclei. [31]

Total characterization can then be defined as relating to the determination of the $\vec{g}$ and $\vec{A}$ tensors in regard to both the isotropic and the anisotropic components.

The isotropic components of the tensors relating to the characterization of the species in question can in general be obtained from the spectrum of the radical species in the liquid phase. In this state the rapid Brownian motion in essence performs a time average, which eliminates the anisotropic components of the tensors leaving just the isotropic component. [31]

The anisotropic components of the tensors relating to the characterization of the species in question can not in general be as easily obtained as the isotropic components.

One experimental method for determining these anisotropic components of the tensors is that relating to the

formation of a paramagnetic species in a single crystal. If a radical can be trapped in a single fixed orientation, or a small number of related orientations, the anisotropic components can, in some cases, be abstracted directly from the spectra. [30], [29] , [22] , [14] , [34] , [17] , [25] , [26] , [37] , [18]

When the radical is trapped in a fixed but randomly distributed orientation in a polycrystalline solid, there is no simple way for abstracting the anisotropic components of the tensors from such spectra. Indeed, only in favorable cases of simple radicals with only one or two tensors and some degree of symmetry has an analysis been completed. [13] , [43] , [20] , [19]

However, recent workers [3] , [21] , [41] , [23] , [24], [28] in the field of polycrystalline studies have devised mathematical schemes to enable one to abstract the anisotropic components from such spectra.

The intention of this investigation was then to select a specific radical species, to attempt to obtain spectra of this species in both the liquid and condensed phases, and finally to find a mathematical scheme by which a total characterization of the species may be made, and which could then be generalized to more complex polycrystalline spectra of short-lived radical species.

The selection of a specific radical species was governed largely by the feasibility of producing the same radical species

in both phases from any particular molecule.

Investigation of the literature reveals that workers have produced a paramagnetic species by decomposition of tetramethyl-2-tetrazene. [36]

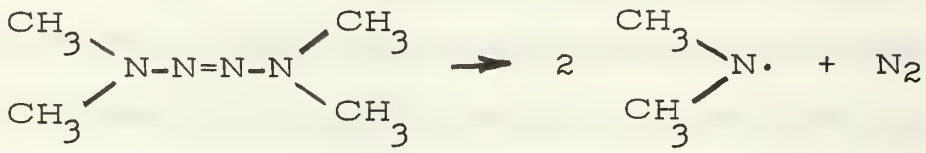

This reaction is particularly attractive, in that only a single radical species is likely to be produced in the condensed phase.

Furthermore, workers have recently devised a scheme to produce short-lived radical species in a flow system by abstracting a hydrogen atom from a large variety of molecules. [8] - [11] The possibility of such a reaction with dimethyl amine would then produce the same radical species in the liquid phase.

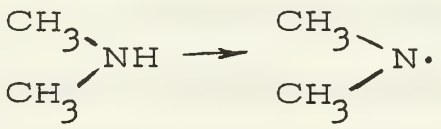

Finally, this radical species has a somewhat unique relationship to a series of radicals which have recently been reported. [12] , [5] , [42] This relationship may be represented as follows:

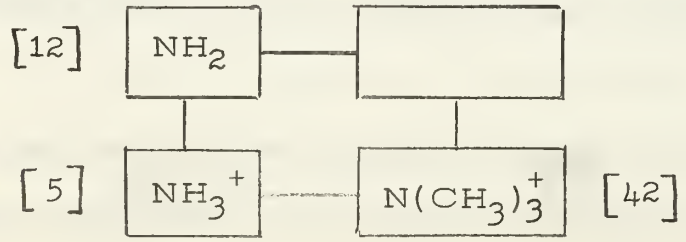

An identification and characterization of the missing radical species would complete the series shown above.

The radical species, dimethyl amidogen, was then selected as the object of this investigation on the basis of the two proposed reaction schemes.

2. Procedure - Flow System

The cell used in the flow system reaction scheme, as shown in Figure 1, was in essence the same as that described by the previous workers. [8] It was constructed locally of quartz in one piece instead of the two-piece design used in the previous work. The width of the flattened portion of the cell was 0.25 mm., which is the optimum dimension when water is used as the solvent, insofar as signal-to-noise ratios are concerned. To obtain a spectrum, a flow rate of approximately 4 ml. per second was found to be required with the above-mentioned cell.

The two reaction solutions were forced through the cell with nitrogen gas at a pressure sufficient to obtain the mentioned rate of flow. The jars containing each of the two solutions were connected to the cell through vinyl tubing with ordinary pinch clamps used to regulate the flow rate. The spectrum could be scanned twice during the passage of four liters total volume through the cell.

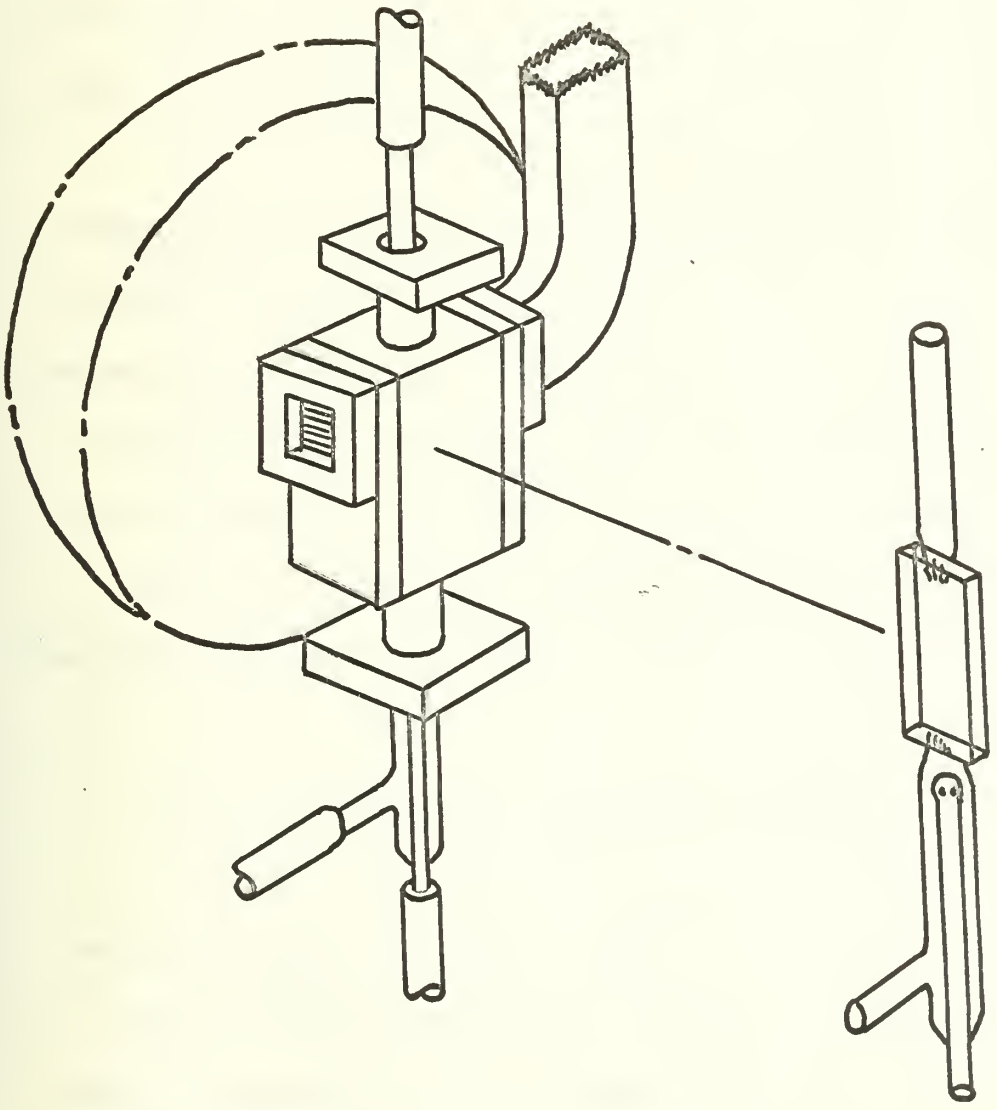

Figure 1

FLOW CELL AND FLOW CELL IN CAVITY

3. Liquid Phase-Flow System

The flow system reaction scheme makes use of the reduction of hydrogen peroxide by transition-metal ions. In this case the titanous ion, which has no observable E.P.R. signal, is oxidized producing hydroxyl radicals.

$$Ti^{3+} + H_2O_2 \rightarrow Ti^{4+} + \cdot OH + OH^-$$

The hydroxyl radical thus produced, abstracts a hydrogen atom from various substances, or, in the case of unsaturated substrates, addition may be possible. [8] - [11]

To ascertain the usefulness of this scheme on molecules of interest in this paper, the published results on the radical derived from methanol was duplicated. The results, shown in Figure 2, agree exactly with those described. [8] The spectrum is assigned to the radical $\cdot CH_2OH$, as evidenced by the triplet, which is due to the coupling with the two carbon protons, and possibly a very weak unresolved coupling with the proton on the oxygen.

Despite the reported absence of radical production by this procedure with ammonia, methyl amine, and triethyl amine [9] an attempt was made to produce a radical species from dimethyl amine. However, no radical species was observed other than the single resonance line attributed to the radical $\cdot OH$ shown in Figure 3, which again agrees with that described. [8] The singlet is observed instead of the expected doublet because of the rapid proton exchange with the water

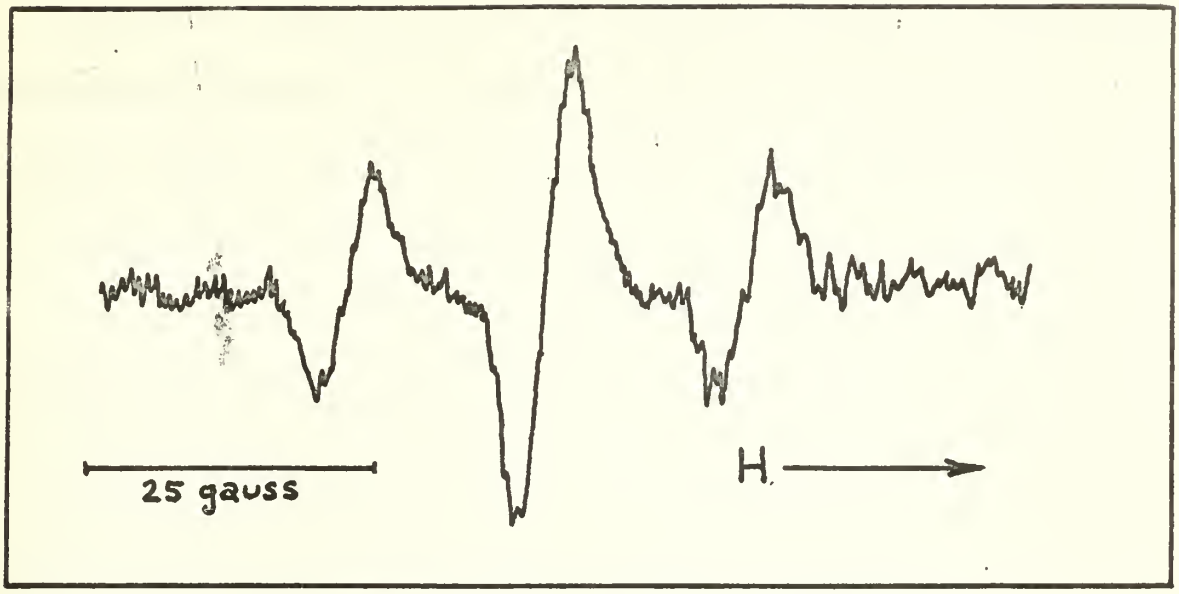

Figure 2 - Radical $\cdot CH_2OH$ with Flow System

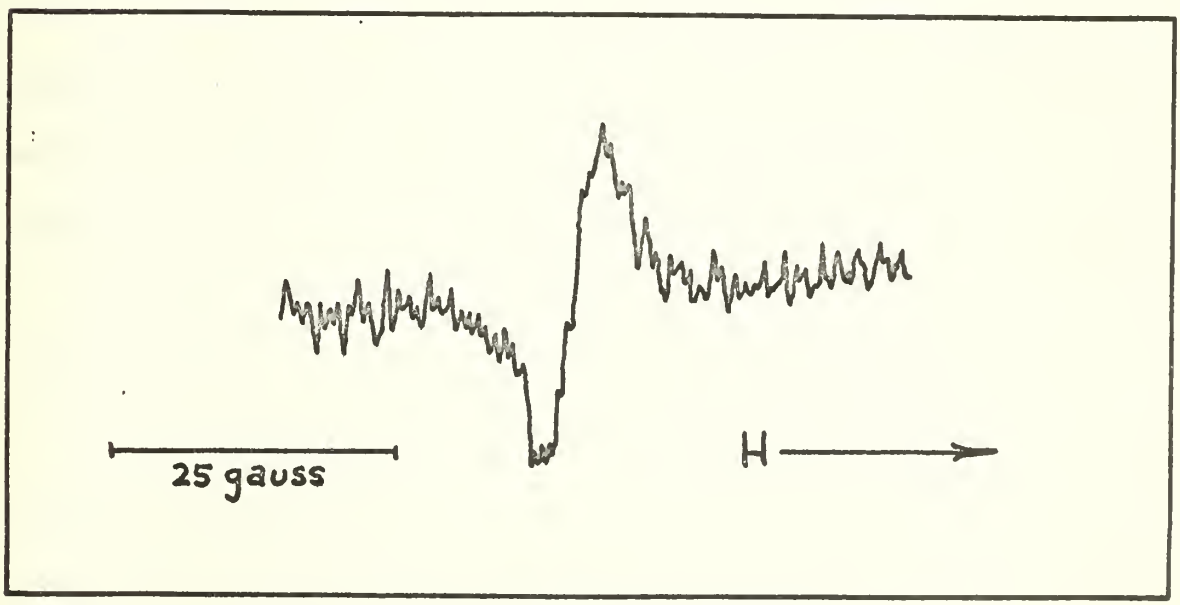

Figure 3 - Radical $\cdot OH$ with Flow System

used as the solvent. It is reported [9] that the simplest amine from which a radical could be produced was n-propyl amine. The proton farthest from the nitrogen is abstracted in this instance.

4. Procedure - Condensed Phase

The procedure by which the radicals of interest were generated in the solid phase was in general the same in all respects, with the exception of the energy source employed to effect the bond cleavage.

The process begins with distilling, under vacuum, approximately 0.2 ml. of the substrate into the bottom finger of the quartz dewar, depicted in Figure 4, at liquid-nitrogen temperatures. The dewar is then filled with liquid nitrogen and the solid sample in the bottom finger is allowed to vaporize and recondense on the finger containing the liquid nitrogen. During the interval in which the sample is in the vapor phase, the energy source is employed so that the radical species is stabilized on the cold finger along with the remaining unreacted substrate. Upon conclusion of the vaporization and recondensation the dewar is transferred to the cavity and the spectrum obtained in a conventional manner.

Spectra were taken on a Varian V-4500 spectrometer with a nine-inch magnet, using 100 kc modulation.

The dewar used was constructed locally of quartz and is of the same design as that obtainable from Varian Associates, with the exception of the stopcock, which is attached by means of a graded glass seal and that it is unsilvered. Under typical circumstances the liquid nitrogen reservoir is sufficient for approximately 20 minutes usage before replenishment is necessary.

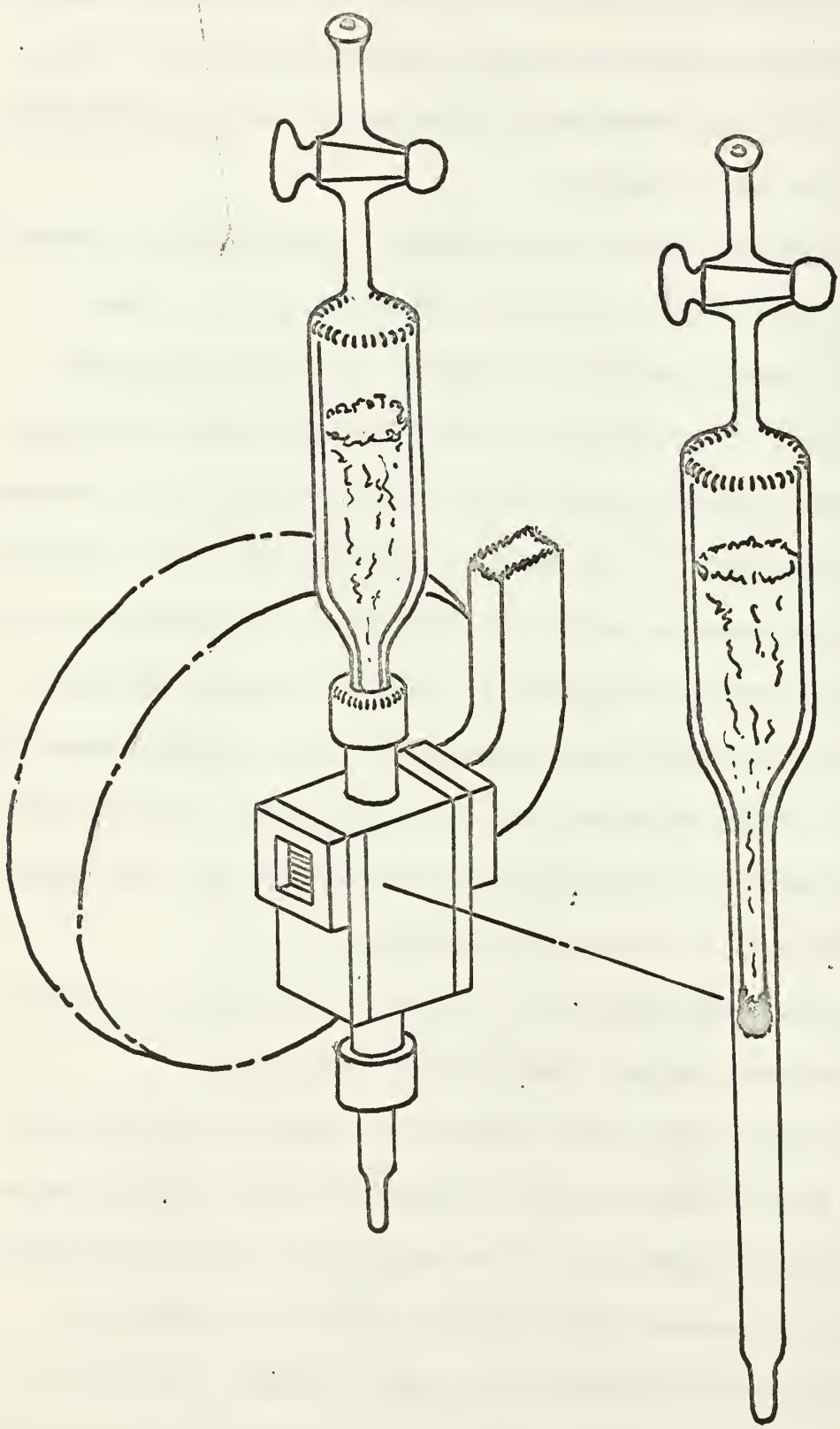

Figure 4

DEWAR AND DEWAR IN CAVITY

The ultraviolet energy source used was a Hanovia Type-S mercury high-pressure lamp with a rated 25.18 watt combined visible-ultraviolet output. This corresponds to approximately 10^{17} Photons/sec. cm^2. at a distance of 0.5 meters. In actual use the lamp was placed as close to the dewar as possible. To reduce the ultraviolet-caused paramagnetic centers in the quartz dewar, a Vycor 7910 filter was used which becomes opaque below approximately 230 millimicrons.

The electrical energy source used was a common laboratory vacuum-testing tesla coil, which was placed adjacent to the dewar at the time the sample passed through the gas phase, the pressure at this time being sufficient to cause an arc.

The $\overleftrightarrow{g}$ tensor values were determined by the use of a known paramagnetic species, 2-2-diphenyl-1-picryl hydrazyl, which has a published g value of 2.00354 ± 0.00003. Very small samples of the crystal were dissolved in benzene and a small quantity placed in a fine capillary. The benzene was allowed to vaporize leaving a minute quantity of the crystal in the capillary which was then sealed.

The sealed capillaries were dropped into the dewar where they settled into the finger when a spectrum of a radical species had been obtained and a g value was desired.

Over a period of time paramagnetic centers appeared in the quartz dewar despite attempts to prevent their formation. These were removed by annealing the finger of the dewar with a hand torch.

5. Condensed Phase - Tesla Coil

It has been proposed that an ordinary tesla coil provides a convenient laboratory tool for producing free radicals in the condensed phase. [32] Among the molecules so examined were CH_3I, CH_3OH, and $(CH_3)_2NH$. No conclusive evidence of a radical species, other than color, was presented and no positive identification of any species was made by the previous workers in this area.

To determine if this process was indeed a practical means of obtaining radicals stabilized in the condensed phase, the molecule CH_3OH was investigated. The tesla coil discharge formed a red-colored condensed phase, yielding the spectrum of Figure 5. This triplet spectrum has been observed by other workers [27] and ascribed to the radical $\cdot CH_2^+$. The coupling observed in this spectrum is consistent with the radical species $\cdot CH_2OH$, the spectrum of which was produced in the flow system and indicated in Figure 2. This previous work produced the radical with X-ray irradiation of the condensed phase.

Similarly, the molecule CH_3I was investigated. The tesla coil discharge formed a rust-colored condensed phase, yielding the spectrum of Figure 6. This quartet spectrum has been observed by many researchers [6] and identified as the radical $\cdot CH_3$. Previous workers produced this radical species with a wide variety of irradiation of a large number of molecules containing the methyl group. The spectrum observed in this investigation is apparently contaminated with another

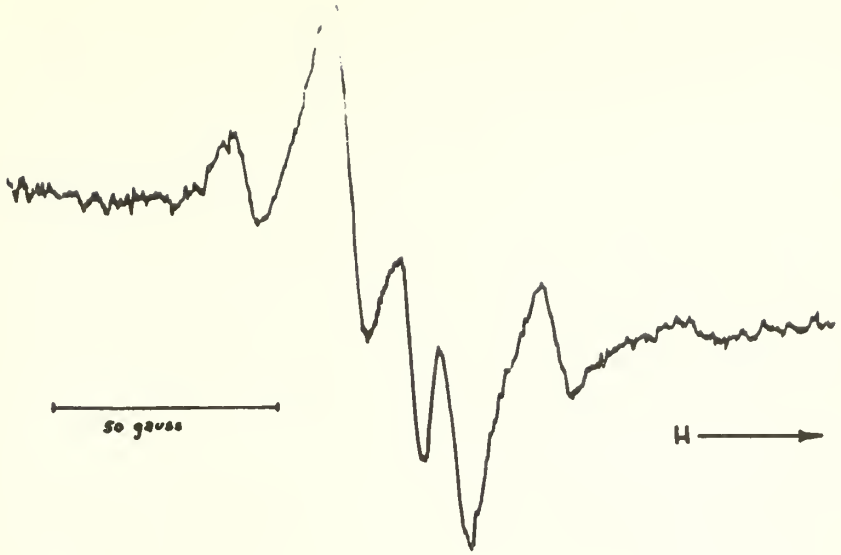

Figure 6 - Tesla Coil Irradiated CH_3I

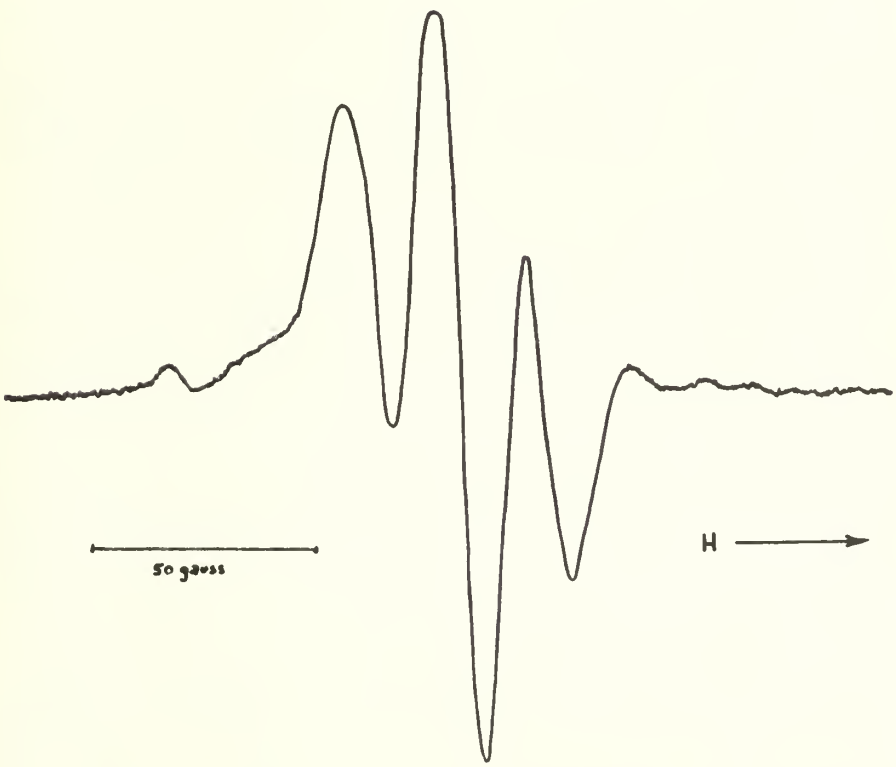

Figure 5 - Tesla Coil Irradiated CH_3OH

paramagnetic species as evidenced by the non-symmetrical singlet superimposed on the quartet. It is likely that this other spectrum line is due to the iodine atom, although this is speculation, as no attempt was made to identify this other species. It was noted that iodine was produced from the process, in that the characteristic violet color of free iodine formed when benzene was used to clean the dewar used in the process.

The molecule $(CH_3)_2NH$ was investigated in the same manner. The tesla coil discharge formed a pale green condensed phase, yielding the spectrum of Figure 7. This rather broad, incompletely resolved, singlet has not previously been identified. Due to the rather small degree of resolution, no assignment of the radical was made in this investigation.

The molecule $(C_6H_5)_2NH$ was investigated in the same manner. The solid $(C_6H_5)_2NH$ was dissolved in benzene at a concentration of 1 molar. The tesla coil discharge did not produce a marked persistant color change; however, a bright blue luminescence appeared from the sample during the discharge of the tesla coil. This luminescence ceased when the discharge was completed. The spectrum shown in Figure 8 was obtained. There is apparently more than a single paramagnetic species present. Due to this complicating factor, no assignment of the radical species was made in this investigation. Other workers [20] have produced a paramagnetic

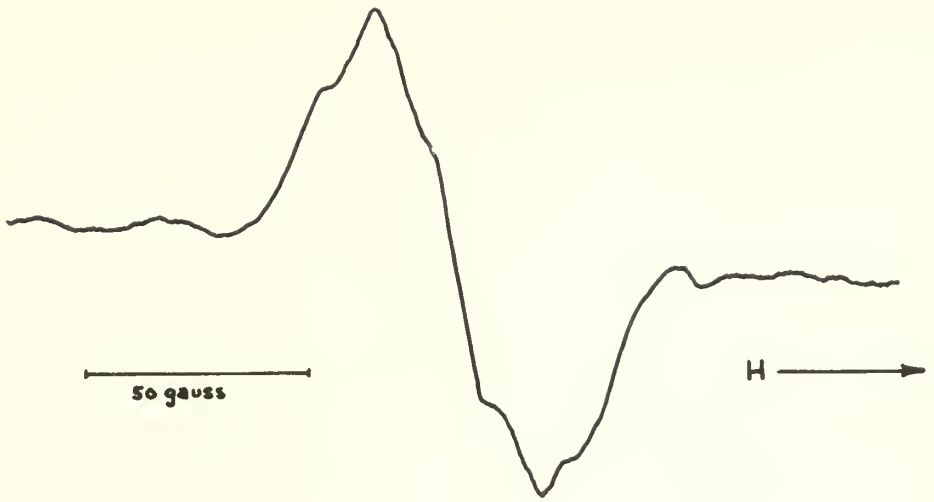

Figure 7 - Tesla Coil Irradiated $(CH_3)_2NH$

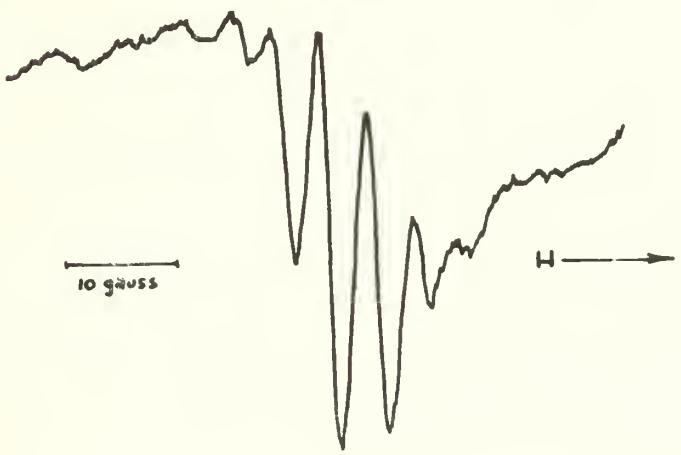

Figure 8 - Tesla Coil Irradiated $(C_6H_5)_2NH$

species from $(C_6H_5)_2NH$ dissolved in toluene in the condenced phase with ultraviolet irradiation and have ascribed the resulting broad, incompletely resolved singlet to the radical $(C_6H_5)_2N$. Furthermore, workers [7] have produced and identified the radical $(C_6H_5)_2N\cdot$ in solution. The spectrum of that species in solution consists of a broad triplet with unresolved hyperfine structure. These same workers [7] have produced a paramagnetic species of tetraphenyl hydrazine in acetic acid which has a five-line spectrum ascribed to $(C_6H_5)_2N_2(C_6H_5)_2^+$ which has a general similarity in appearance with that produced in this investigation.

The molecule CH_3NH_2 was investigated in the same manner. The tesla coil discharge did not produce a marked persistent color change. The spectrum shown in Figure 9 was obtained. This broad, unresolved singlet has been observed but has not been ascribed to a radical species by previous workers. [27] Due to the lack of structure, no assignment of the radical species was made in this investigation.

The molecule $(C_2H_5)_2NH$ was investigated in the same manner. The tesla coil discharge did not produce a marked persistent color change. The spectrum shown in Figure 10 was obtained. This broad, unresolved singlet has not been reported; however, previous workers [27] have observed a similar broad singlet resulting from the X-ray irradiation of ethyl amine. Due to the lack of structure, no assignment of

Figure 10 - Tesla Coil Irradiated $(C_2H_5)_2NH$

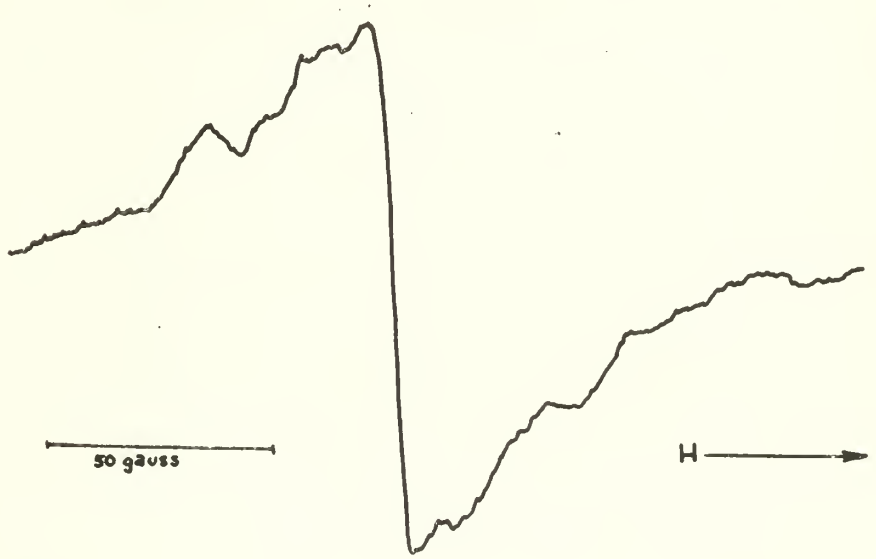

Figure 9 - Tesla Coil Irradiated CH_3NH_2

radical species was made in this investigation.

The molecule NH_3 was investigated in the same manner to complete the series of simple nitrogen-containing compounds. The tesla coil discharge produced a blue-colored condensed phase, yielding the spectrum of Figure 11. Previous workers [12] have produced the radical $\cdot NH_2$ by ultraviolet irradiation of the NH_3 condensed phase in an argon matrix at 4°K. The spectrum obtained in this investigation, although similar, has somewhat broader lines and a somewhat different intensity distribution. However, the hyperfine structure may permit an analysis based on the Hamiltonian for such a system. Subject to such an analysis the radical species is tentatively identified as $\cdot NH_2 \cdot$

Tetramethyl tetrazene was investigated by the same procedure to provide some correlation between the paramagnetic species so formed, with the paramagnetic species formed by the photolysis of the same substrate, as discussed elsewhere in this report. The spectrum so obtained consisted of more than a single radical species as shown in Figure 12. The primary radical species present is identical with that obtained by photolysis; however, there is another paramagnetic species present. The principle radical is identified as dimethyl amidogen. No attempt to identify the second radical was made.

At this juncture it might be pointed out that the first section of the investigation has been shown to be at least

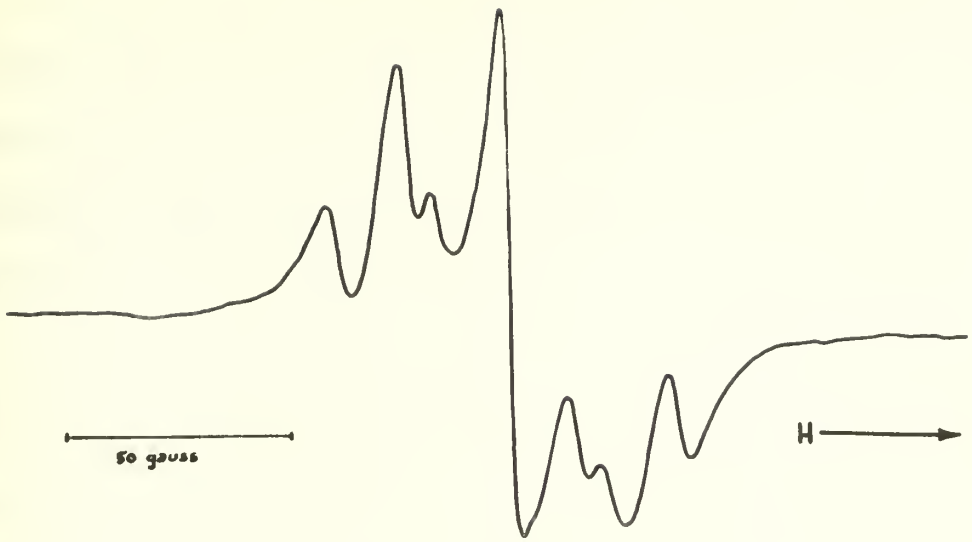

Figure 11 - Tesla Coil Irradiated NH_3

Figure 12 - Tesla Coil Irradiated $(CH_3)_2N-N=N-N(CH_3)_2$

feasible. The molecule CH_3OH has yielded a radical species whose spectra consists of a triplet in the ratio of 1:2:1 in both liquid and condensed phases. The condensed phase spectra consists of lines which exhibit the broadening characteristic of the anisotropies in the related tensors while the liquid phase spectra apparently exhibits only the isotropic components.

6. Condensed Phase - Ultraviolet

It has been reported [36] that a violet, paramagnetic solid forms when tetramethyl tetrazene vapor is subjected to ultraviolet irradiation and subsequently condensed on a liquid nitrogen-cooled surface. These workers have concluded that this paramagnetic species is dimethyl amidogen or the dimethyl amino radical, although there was no positive identification of that radical species. Other workers [40] photolyzed tetramethyl tetrazene in a similar manner and found evidence for a radical species of the type $(CH_3)_2N_3$ based on ultraviolet-visible spectroscopy.

Samples of tetramethyl tetrazene were subjected to ultraviolet irradiation as described elsewhere in this paper and and E.P.R. spectrum of the radical species is shown in Figures 13 and 14.

Similar attempts to produce radical species with dimethyl amine, diphenyl amine, and diethyl amine proved fruitless by this procedure.

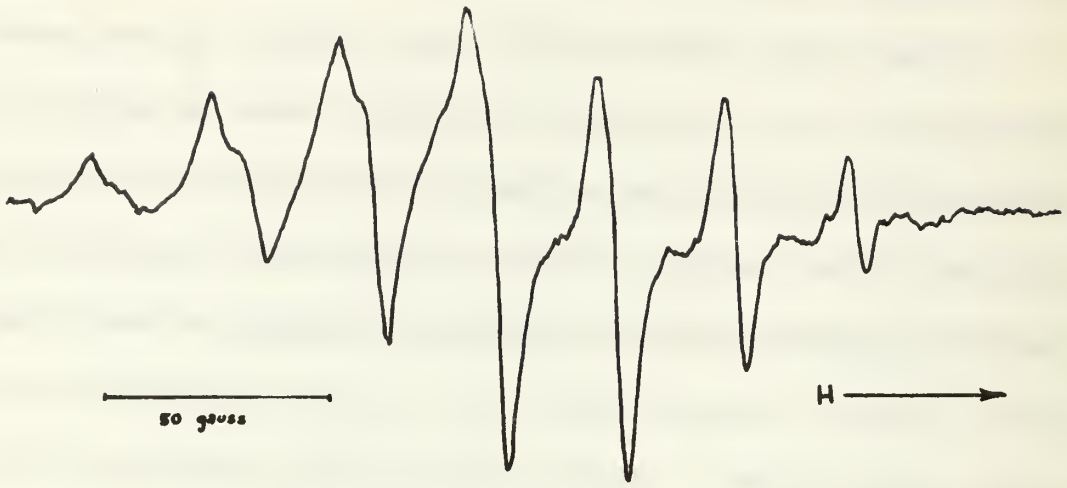

Figure 13 - Ultra-Violet Irradiated $(CH_3)_2$-N-N=N-N $(CH_3)_2$

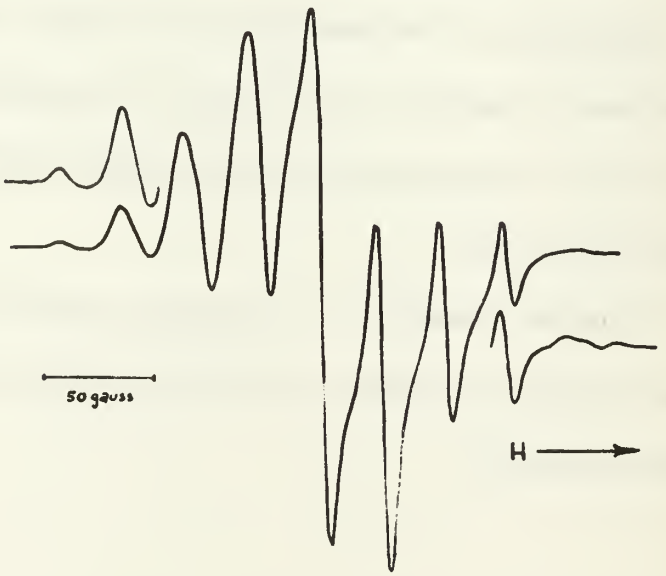

Figure 14 - Ultra-Violet Irradiated $(CH_3)_2$-N-N=N-N $(CH_3)_2$
(Higher Signal Level in Wings)

7. Polycrystalline Line Shapes

It can be shown that the anisotropic components of the $\overleftrightarrow{g}$ and $\overleftrightarrow{A}$ tensors are averaged to zero when the paramagnetic species is subjected to a rapid Brownian tumbling motion leaving just the isotropic components of the tensors. [31] In all other situations, the anisotropic component is responsible for the orientation-dependent interactions which are observed in E.P.R. spectra. These orientation-dependent interactions are often the dominant features in spectra dealing with single crystals. Glassy or polycrystalline solids feature spectra which are statistical averages of the anisotropic interactions.

In principle the interpretation of E.P.R. spectra in polycrystalline solids could be resolved by the direct application of the spin Hamiltonian of the system under consideration. This approach is hampered by the magnitude of the calculations involved. Consider for example, the diagonalization of a 42 x 42 matrix of complex numbers, not once, but a number of times, approximating all possible orientations of the radical with respect to some axis system. This entire process would have to be repeated for an indefinite period of time if no knowledge of the tensors was available other than just the polycrystalline spectra. In general, there is no simple way for obtaining the parameters of the spin Hamiltonian by analysis of a line shape.

In view of the magnitude of the problem, workers in this field have tended to limit the scope of the problem to simpler

systems. For example -CH- fragments, where the system is limited to 1 proton. [3] , [41] , [23] Others have limited the scope of the problem to just the $\overleftrightarrow{g}$ tensor anisotropies. [21], [28]

Recently one of these workers [24] completed a most comprehensive mathematical scheme for the interpretation of polycrystalline spectra for a large range of paramagnetic systems. This calculation is performed on a digital computer and thus provides the technical possibility of performing the calculation for the line shapes to be expected from the anisotropic interactions in a polycrystalline solid.

Although a detailed description of the mathematical scheme used by Lefebvre and Maruani [24] is not essential to this investigation, a brief summary of the calculation may provide some general background for the analysis which follows.

The Hamiltonian presented in the introduction does not contain all the terms responsible for the shape of the E.P.R. spectra; however, most of the neglected terms may roughly be taken into account by broadening the lines calculated with the effective Hamiltonian. As an approximation, this broadening may be taken as independent of the component line and of the radical orientation. Experiments on monocrystals have shown that the component lines are essentially Gaussian-shaped in nature.

The monocrystal component line shape, $F_\lambda(H, \Theta_0, \Phi_0)$, can then be written

$$F_k(H,\Theta_0,\Phi_0) = \left(\frac{1}{\lambda}\right)\left(\frac{2}{\pi}\right)^{\frac{1}{2}} e^{-2\left[H - H_k(\Theta_0,\Phi_0)\right]^2/\lambda^2}$$

where λ is the line width; H the magnitude of the magnetic field; Θ_0 and Φ_0 the angles specifying the orientation of the magnetic field with respect to the reference system of axes; H_k the magnetude of the magnetic field at the resonance condition for the component line.

The monocrystalline over-all line shape is the weighted superposition of all the component line shapes

$$F(H,\Theta_0,\Phi_0) = \frac{1}{N_r} \sum_{k=1}^{M_r} F_k(H,\Theta_0,\Phi_0)\ I_k(\Theta_0,\Phi_0)$$

where;

$$N_r = \prod_{i=1}^{M_n} (2I_i+1) \qquad \text{and} \qquad M_r = \prod_{i=1}^{M_n} (2I_i+1)^2$$

are the normalizing factors and summation limit for a total of M_n magnetic nuclei.

To obtain the derivative spectrum, all the components have to be derived separately, and their expressions multiplied by the factor:

$$-\left(\frac{4}{\lambda}\right)^2 \left[H - H_k(\Theta_0,\Phi_0)\right]$$

The $H_k(\Theta_0,\Phi_0)$ the magnetic field corresponding to the component line, can be obtained by a series of summations of "shifts" in field units corresponding to the effects of the various tensors. These shifts are in relation to the free electron resonant field, which in turn is dependent on the operating frequency of the spectrometer.

The effective $\vec{\vec{g}}$ shift can be expressed in terms of θ_g and Φ_g, the angles which relate the magnetic field to the principal axes of the tensor;

$$H_e' - H_e = -H_e\left(\epsilon_x \sin^2\theta_g \cos^2\Phi_g + \epsilon_y \sin^2\theta_g \sin^2\Phi_g + \epsilon_z \cos^2\theta_g\right)$$

where H_e' is the electron resonance field with $\vec{\vec{g}}$ tensor anisotropy present, and H_e is the electron resonance field without anisotropy present. The terms are defined by;

$$\epsilon_{x,y,z} = \frac{g_{x,y,z}}{g_0} - 1$$

where 2.0023 is the value of g_0, or that corresponding to the free electron.

The hyperfine shift may be expressed in terms of θ_i and Φ_i the angles which relate the magnetic field to the principal axes of each of the $\vec{\vec{A}}_i$ tensors.

This shift is symmetric with respect to the frequency corresponding to H_e', where the conversion between field units and frequency is:

$$h\nu_i = g_{ni}\beta_n H_i$$

The shift, in terms of a coupled sign convention, to include both the up and down field component line may be expressed as:

$$\nu_i'^{\pm} = \left[\left(\nu_i \mp \tfrac{1}{2}a_i^x\right)^2 \sin^2\theta_i \cos^2\Phi_i + \left(\nu_i \mp \tfrac{1}{2}a_i^y\right)^2 \sin^2\theta_i \sin^2\Phi_i + \left(\nu_i \mp \tfrac{1}{2}a_i^z\right)^2 \cos^2\theta_i\right]^{\frac{1}{2}}$$

Here ν_i represents the resonance frequency of the free nucleus, and ν_i' represents the effective frequency of the nucleus. The a_i represent the principal values of the hyperfine coupling tensor.

The $I_k(\theta_0, \Phi_0)$, the intensities corresponding to the component line, can be obtained from the elements of a Wigner matrix.

This matrix is expressed as a function of the angle ξ_i, of rotation of the quantization axis of the nuclear spin, I_i, when an electron spin transition occurs.

This angle ξ_i is given by;

$$\cos \xi_i = \frac{\nu_i^2 - \frac{1}{4}(a_{xi}^2 \sin^2\theta_i \cos^2\phi_i + a_{yi}^2 \sin^2\theta_i \sin^2\phi_i + a_{zi}^2 \cos^2\theta_i)}{(\nu_i'^{+})(\nu_i'^{-})}$$

where the terms here have their previous definitions.

The matrix of elements is given by the Wigner relation;

$$r_{M_i M_i'}^{(I_i)} = \sum_t (-1)^t \frac{\left[(I_i+M_i)!(I_i-M_i)!(I_i+M_i')!(I_i-M_i')!\right]^{\frac{1}{2}}}{(I_i+M_i-t)!(I_i-M_i'-t)!(t-M_i+M_i')!}$$

$$\times \left[\cos\frac{\xi_i}{2}\right]^{2I_i+M_i-M_i'-2t} \left[\sin\frac{\xi_i}{2}\right]^{2t-M_i+M_i'}$$

Where M_i and M_i' are two of the possible $2I_i+1$ quantum states of the nuclear spin I_i. The summation is over all integral values of t for which the factorials are defined.

Now for a polycrystalline sample, the absorption at each point in the spectrum is the superposition of all the absorptions from all component lines at that point for all of the randomly distributed orientations. This may be expressed:

$$F(H) = \frac{1}{4\pi} \int_0^{2\pi} d\Phi_0 \int_0^{\pi} F(H, \theta_0, \Phi_0) \sin\theta_0 \, d\theta_0$$

The integration of this expression is not possible by analytical means due to the form of the expressions for the individual component line shapes. The numerical integration has to be made only on half of the sphere for symmetry reasons. When all of the tensors have one common axis the integration can be limited to a quarter of the sphere, and when the tensors have all axes in common the integration can be restricted

to an eighth of the sphere. [24]

The digital computer program referred to in the previously mentioned paper concerning polycrystalline spectra [21] was obtained from the Library of Congress, Document Number 8275.

After translation of the original French Fortran into the compatible English version and some modification to permit its use on the CDC 1604, the program seemed to perform satisfactorily with the exception of the computer time required to complete a calculation.

Typically, one of the following calculations required 20 minutes of computer time. This excessive time requirement was later reduced to 5 minutes for the equivalent computation by the use of the newer Fortran routine now available.

To ascertain that the modified computer routine was, in fact, capable of calculating the polycrystalline spectra satisfactorily, a verification of the reported [19] radical FOO· was completed. This calculation also determined in general, a background for the number of orientations required in the calculation and a general background for the effect of the line-width parameter.

Figure 15 is an indication of the effect of increasing the line-width parameter. The detailed line shapes and other small irregularities wash out, resulting in a quite different spectrum.

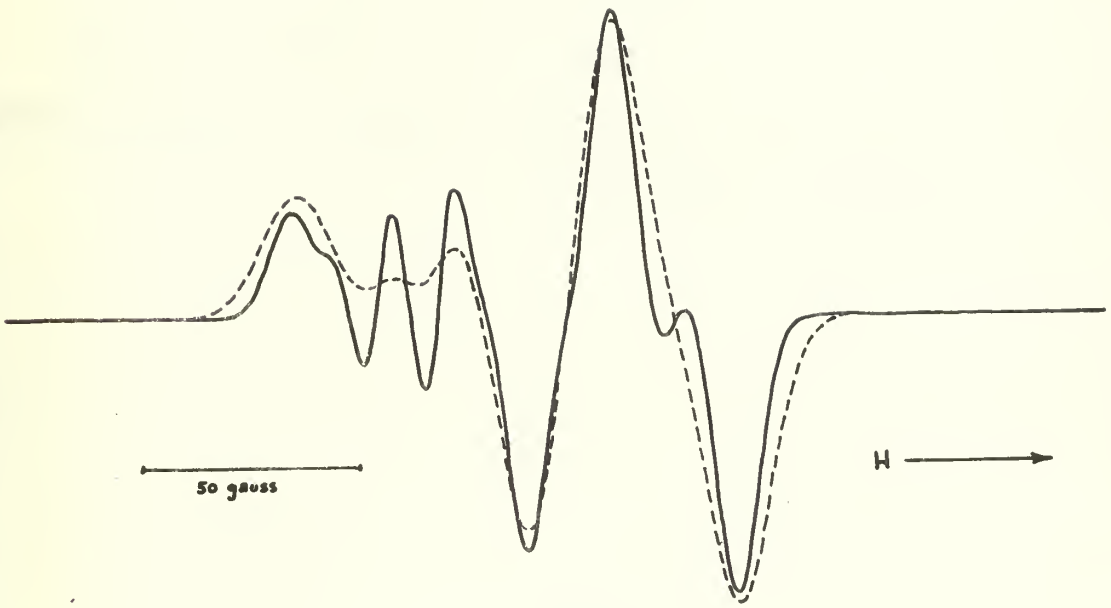

Figure 15
FOO· RADICAL FROM O_2F_2

SOLID LINE	DASHED LINE
8 ORIENTATIONS	8 ORIENTATIONS
5 G LINE WIDTH	7 G LINE WIDTH

THESE CALCULATED SPECTRA INDICATE THE EFFECT OF CHANGING THE LINE WIDTH PARAMETER. THIS INDICATES THE NECESSITY OF NOT USING TOO WIDE A COMPONENT LINE AS THIS MAY WASH OUT FEATURES VITAL TO THE PROPER RECONSTRUCTION OF A SPECTRUM

Figure 16 is an indication of the necessity for using an adequate number of orientations in the calculation. The difference between the two spectra is marked and is due solely to increasing the number of orientations, in this case, from 8 to 16. It also must be remembered that the computer time increases rapidly with the number of orientations. Therefore, the number of orientations used should be no more than necessary to reproduce the spectra in question.

This last spectrum is completely consistent with the observed spectrum and demonstrates that the computer routine produces satisfactory calculations.

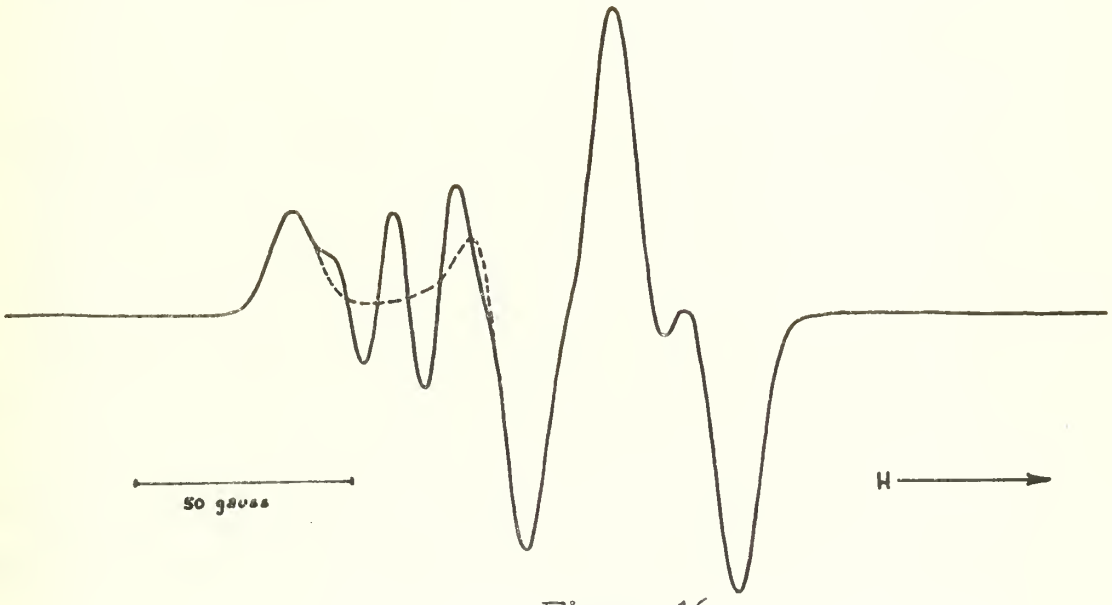

Figure 16

FOO· RADICAL FROM O_2F_2

SOLID LINE	DASHED LINE
8 ORIENTATIONS	16 ORIENTATIONS
5 G LINE WIDTH	5 G LINE WIDTH

THESE CALCULATED SPECTRA INDICATE THE EFFECT OF CHANGING THE NUMBER OF ORIENTATIONS USED IN THE SUMMATION. THIS DEMONSTRATES THE NECESSITY OF USING A SUFFICIENT NUMBER OF ORIENTATIONS. THE DASHED LINE REPRODUCES THE EXPERIMENTAL SPECTRUM EXACTLY.

8. Interpretation

Once reproducible E.P.R. spectra were obtained from the photolysis of tetramethyl tetrazene, it appeared to be possible to conduct a mathematical analysis from the polycrystalline spectrum, despite the lack of a spectrum of the radical in the liquid phase. The hyperfine structure seemed to be totally resolved and the spectrum could be explained on the basis of six equivalent protons, each with spin of one-half and one nitrogen atom with spin of one.

Such a reconstruction is on the basis of approximately equal proton and nitrogen coupling tensors. The resulting stick diagram is indicated in Figure 17, each of the three seven-line spectra representing the six equivalent protons. The intensities of these seven lines are in the ratio of 1:6:15:20:15:6:1. The superimposed or resulting spectrum has a nine-line pattern with intensities in the ratio of 1:7:22:41:50:41:22:7:1.

The experimental spectrum of the paramagnetic species was re-examined in an attempt to ascertain if indeed there were two additional lines in the wings. Figure 14 is the spectrum obtained which demonstrates the existence of the total nine-line spectrum.

At this juncture an attempt was made to correlate the rough couplings, based on the previous assumption, with the values of the tensors of the related radicals, NH_2, [12]

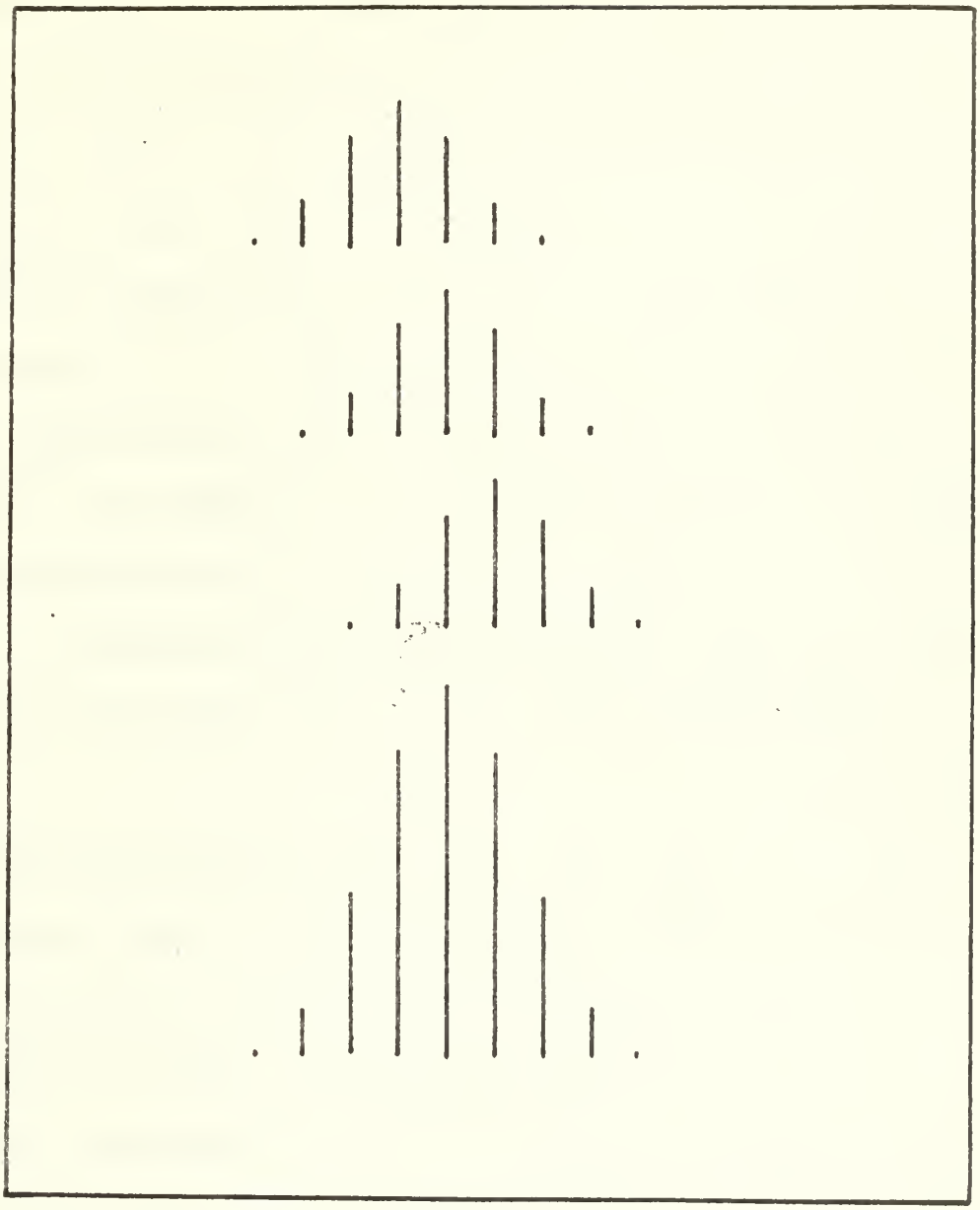

Figure 17
RECONSTRUCTED FIRST ORDER STICK SPECTRUM OF DIMETHYL AMIDOGEN, $(CH_3)_2N\cdot$

NH_3^+, [5] and $N(CH_3)_3^+$. [42] This approach proved fruitless, in that there is little or no correlation in the values of the nitrogen coupling tensors in the series. However, there seemed to be some degree of rotation associated with each of the other species leading to axial symmetry of the tensors.

Therefore, the assumption was made that if the paramagnetic species were indeed dimethyl amidogen it would most probably exhibit axial symmetry as well. In this manner only two axes, the so-called parallel and the perpendicular, are required to specify the tensors characterizing the coupling involved in the radical, instead of the three which would normally be required in the absence of such symmetry.

Consequently, a list of the variables involved in the calculation are:

$g_{\parallel}$ $g_{\perp}$ $A^N_{\parallel}$ $A^N_{\perp}$ $A^H_{\parallel}$ $A^H_{\perp}$ and the line-width.

More generally, in the initial phases of the calculations, the exact values of each of these variables will not be essential toward reconstructing the spectrum; rather it will be the relative values of the parallel and the perpendicular components which will control the relative shape and location of each line in the spectrum.

Therefore, the variables involved in the following calculations are:

$$\frac{g_{\parallel}}{g_{\perp}}, \quad \frac{A^N_{\parallel}}{A^N_{\perp}}, \quad \frac{A^H_{\parallel}}{A^H_{\perp}}, \quad \frac{A^N \text{ isotropic}}{A^H \text{ isotropic}}$$

The line-width can be determined directly from the high field side of the experimental spectrum. A value of 5 gauss was used in the calculations.

Although, in general, it would be impossible to correlate to each feature, in each component line, the corresponding anisotropic interaction, it may be helpful to keep in the background the general effect of such anisotropies. Figure 18 indicates such a generalized effect on a seven-line spectrum which might arise from a system containing six equivalent protons. The first stick figure might represent the spectrum resulting from a given orientation of the radical which can be used as a reference for any other orientation. The second line represents the spectrum resulting from another orientation of the radical with respect to the first. In this second orientation, the $\overrightarrow{\overrightarrow{g}}$ tensor anisotropy is such that the spectrum is shifted uniformly to the left. The magnitude and direction of this shift is just illustrative and may equally be opposite to that indicated. Likewise, in this orientation the individual component lines are shifted outward from the center of the spectrum due to the anisotropy in the hyperfine coupling tensor. Here again the magnitude and direction are illustrative only and may be opposite to that indicated. The resulting spectrum from these two orientations is represented in the third stick spectrum. This general effect of broadening and narrowing of the line-widths is typical of

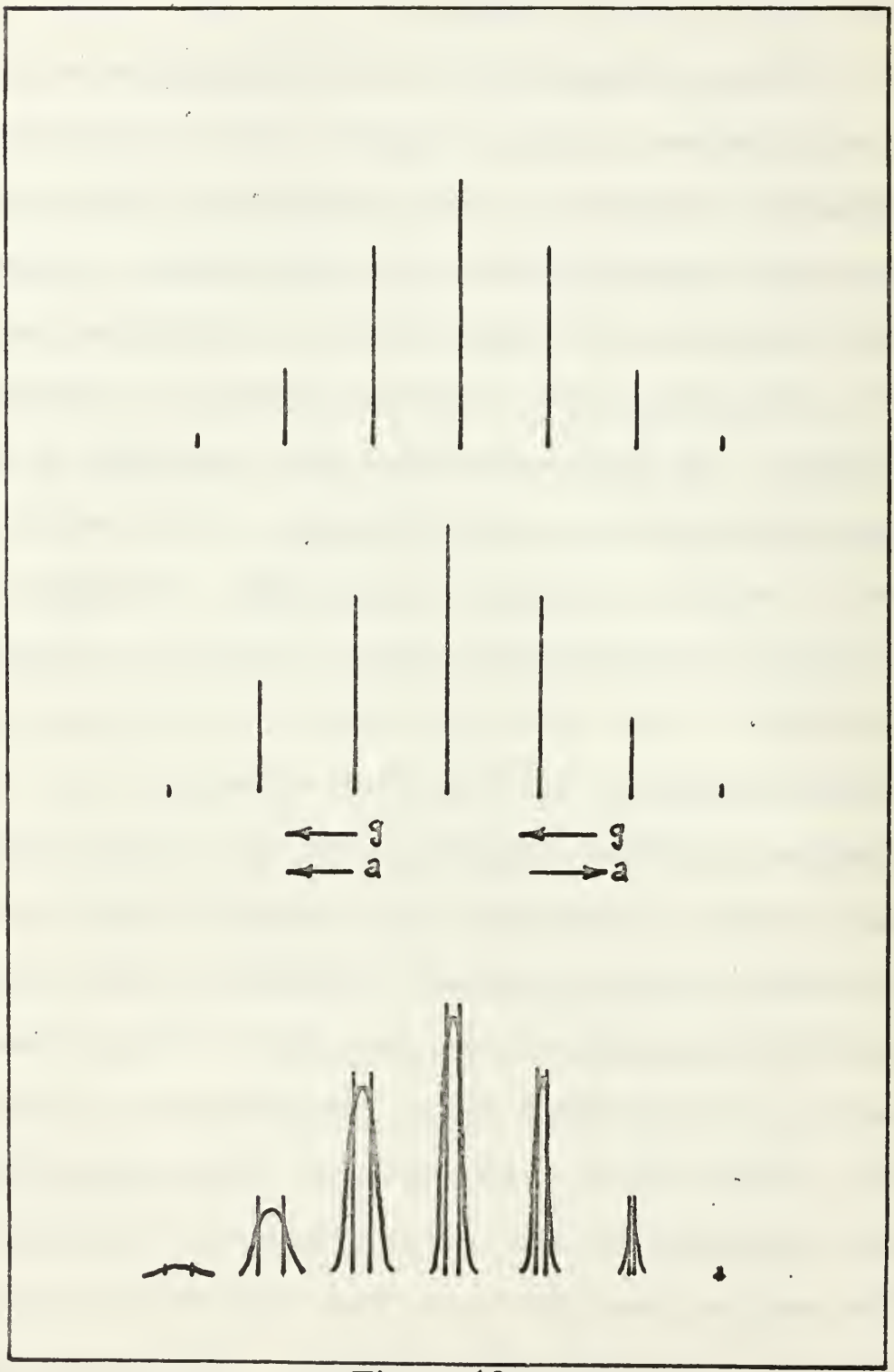

Figure 18

DIAGRAM REPRESENTING THE EFFECT OF ANISOTROPIC COMPONENTS IN THE TENSORS

the anisotropies of the related tensors.

The subsequent series of figures typically represent a part of the library which was formed by use of the previously mentioned digital computer routine. Each of the variables was introduced and changed in sequence to provide a basis upon which final determination of the characterization of dimethyl amidogen could be made.

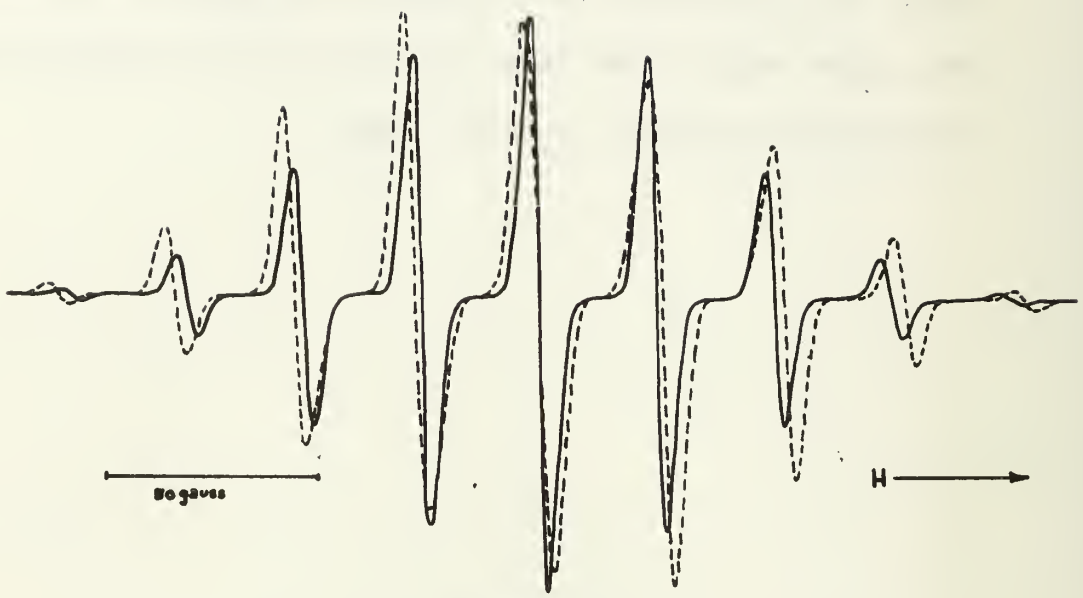

Figure 19
DIMETHYL AMIDOGEN, $(CH_3)_2N\cdot$

SOLID LINE	DASHED LINE
$A_{\parallel}^{N} = 27.4$ G	$A_{\parallel}^{N} = 30.4$ G
$A_{\perp}^{N} = 27.4$ G	$A_{\perp}^{N} = 30.4$ G
$A_{\parallel}^{H} = 27.4$ G	$A_{\parallel}^{H} = 27.4$ G
$A_{\perp}^{H} = 27.4$ G	$A_{\perp}^{H} = 27.4$ G
$g_{\parallel} = 2.0042$	$g_{\parallel} = 2.0042$
$g_{\perp} = 2.0042$	$g_{\perp} = 2.0042$

THESE CALCULATED SPECTRA INDICATE THE CHANGE WHICH OCCURS WHEN THE RATIO A^N ISOTROPIC/A^H ISOTROPIC IS INCREASED, ALL OTHER PARAMETERS REMAINING CONSTANT.

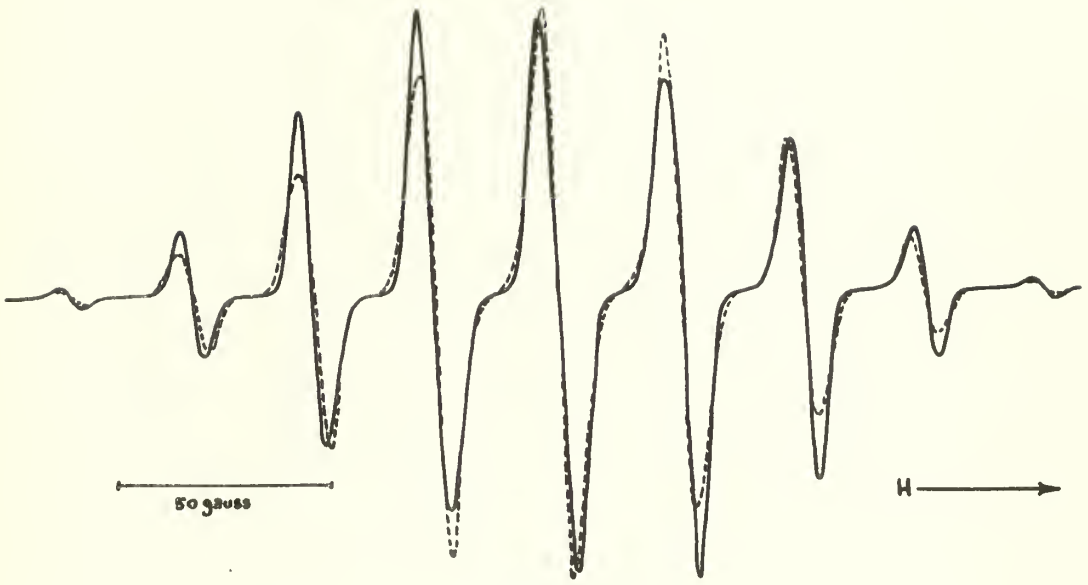

Figure 20

DIMETHYL AMIDOGEN, $(CH_3)_2N$

SOLID LINE	DASHED LINE
$A_{\parallel}^{N} = 30.4$ G	$A_{\parallel}^{N} = 34.2$ G
$A_{\perp}^{N} = 30.4$ G	$A_{\perp}^{N} = 28.4$ G
$A_{\parallel}^{H} = 27.4$ G	$A_{\parallel}^{H} = 27.4$ G
$A_{\perp}^{H} = 27.4$ G	$A_{\perp}^{H} = 27.4$ G
$g_{\parallel} = 2.0042$	$g_{\parallel} = 2.0042$
$g_{\perp} = 2.0042$	$g_{\perp} = 2.0042$

THESE CALCULATED SPECTRA INDICATE THE CHANGE WHICH OCCURS WHEN THE RATIO $A_{\parallel}^{N}/A_{\perp}^{N}$ IS INCREASED, ALL OTHER PARAMETERS REMAINING CONSTANT.

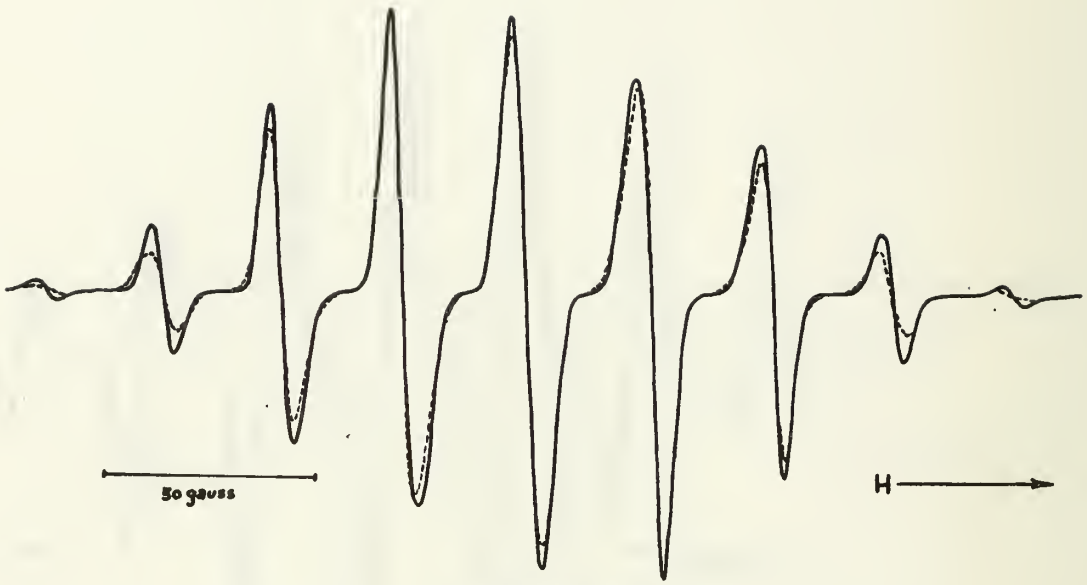

Figure 21

DIMETHYL AMIDOGEN, $(CH_3)_2N\cdot$

SOLID LINE	DASHED LINE
$A_{\parallel}^{N}$ = 30.4 G	$A_{\parallel}^{N}$ = 30.4 G
$A_{\perp}^{N}$ = 30.4 G	$A_{\perp}^{N}$ = 30.4 G
$A_{\parallel}^{H}$ = 27.4 G	$A_{\parallel}^{H}$ = 29.6 G
$A_{\perp}^{H}$ = 27.4 G	$A_{\perp}^{H}$ = 26.4 G
$g_{\parallel}$ = 2.0042	$g_{\parallel}$ = 2.0042
$g_{\perp}$ = 2.0042	$g_{\perp}$ = 2.0042

THESE CALCULATED SPECTRA INDICATE THE CHANGE WHICH OCCURS WHEN THE RATIO OF $A_{\parallel}^{H}/A_{\perp}^{H}$ IS INCREASED, ALL OTHER PARAMETERS REMAINING CONSTANT.

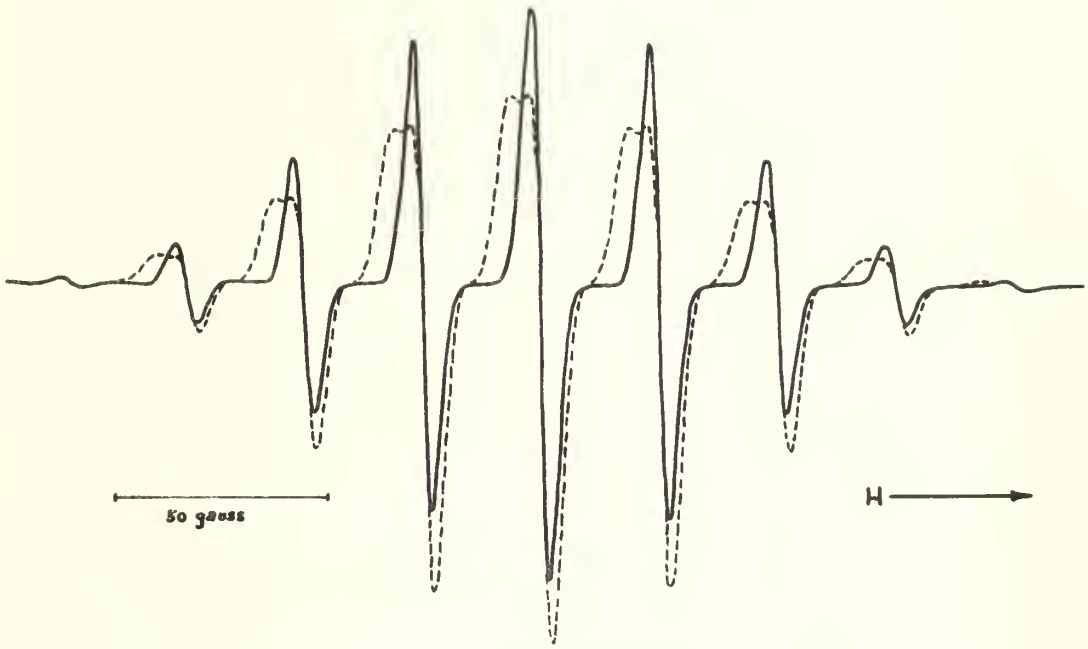

Figure 22
DIMETHYL AMIDOGEN, $(CH_3)_2N\cdot$

SOLID LINE	DASHED LINE
$A_{\parallel}^{N} = 27.4$ G	$A_{\parallel}^{N} = 27.4$ G
$A_{\perp}^{N} = 27.4$ G	$A_{\perp}^{N} = 27.4$ G
$A_{\parallel}^{H} = 27.4$ G	$A_{\parallel}^{H} = 27.4$ G
$A_{\perp}^{H} = 27.4$ G	$A_{\perp}^{H} = 27.4$ G
$g_{\parallel} = 2.0042$	$g_{\parallel} = 2.0098$
$g_{\perp} = 2.0042$	$g_{\perp} = 2.0042$

THESE CALCULATED SPECTRA INDICATE THE CHANGE WHICH OCCURS WHEN THE RATIO OF $g_{\parallel}/g_{\perp}$ IS INCREASED, ALL OTHER PARAMETERS REMAINING CONSTANT.

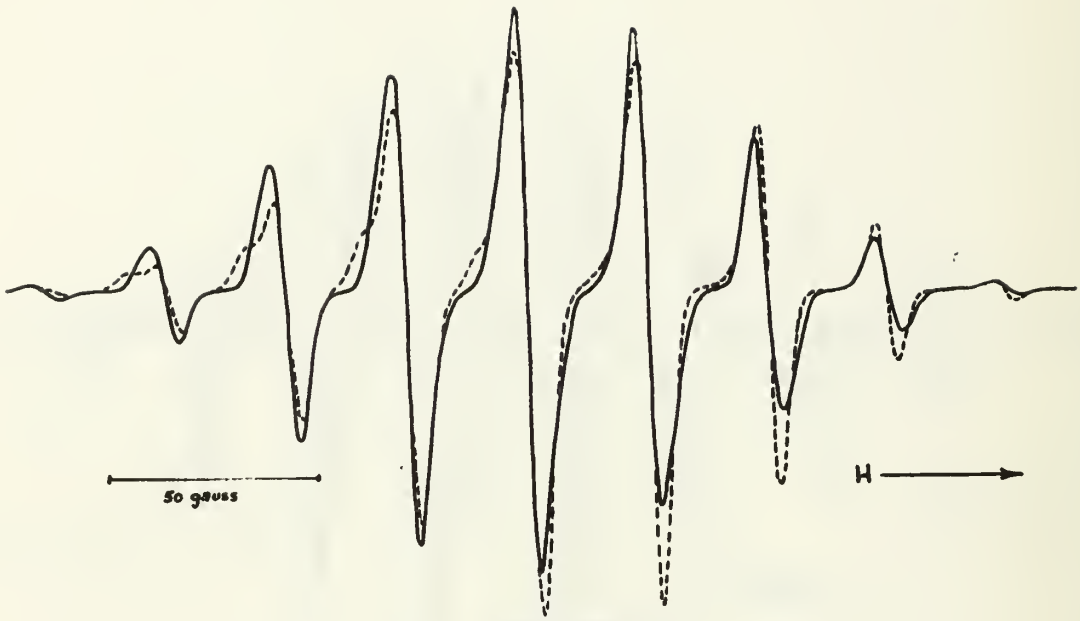

Figure 23
DIMETHYL AMIDOGEN, $(CH_3)_2N\cdot$

SOLID LINE	DASHED LINE
$A_{\parallel}^{N}$ = 34.2 G	$A_{\parallel}^{N}$ = 34.2 G
$A_{\perp}^{N}$ = 28.5 G	$A_{\perp}^{N}$ = 28.5 G
$A_{\parallel}^{H}$ = 27.4 G	$A_{\parallel}^{H}$ = 27.4 G
$A_{\perp}^{H}$ = 27.4 G	$A_{\perp}^{H}$ = 27.4 G
$g_{\parallel}$ = 2.0042	$g_{\parallel}$ = 2.0071
$g_{\perp}$ = 2.0042	$g_{\perp}$ = 2.0042

THESE CALCULATED SPECTRA INDICATE THE CHANGE WHICH OCCURS WHEN THE RATIO $g_{\parallel}/g_{\perp}$ IS INCREASED WHILE ANISOTROPIC NITROGEN COUPLING AND ISOTROPIC HYDROGEN COUPLING EXISTS.

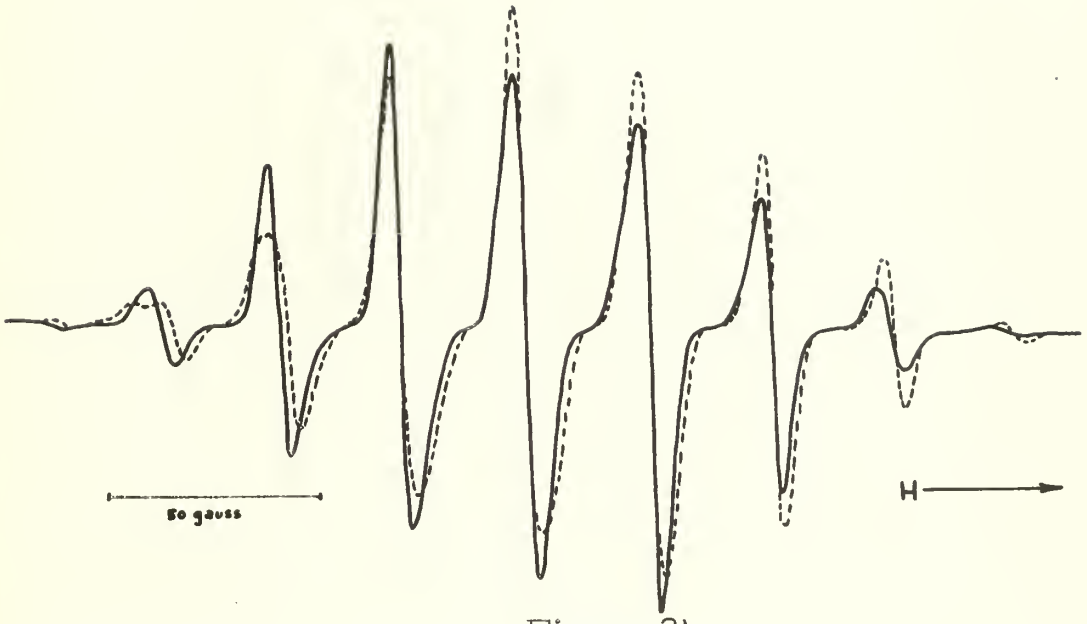

Figure 24

DIMETHYL AMIDOGEN, $(CH_3)_2N\cdot$

SOLID LINE	DASHED LINE
$A_{\parallel}^{N} = 30.4$ G	$A_{\parallel}^{N} = 30.4$ G
$A_{\perp}^{N} = 30.4$ G	$A_{\perp}^{N} = 30.4$ G
$A_{\parallel}^{H} = 29.4$ G	$A_{\parallel}^{H} = 29.4$ G
$A_{\perp}^{H} = 26.4$ G	$A_{\perp}^{H} = 26.4$ G
$g_{\parallel} = 2.0042$	$g_{\parallel} = 2.0071$
$g_{\perp} = 2.0042$	$g_{\perp} = 2.0042$

THESE CALCULATED SPECTRA INDICATE THE CHANGE WHICH OCCURS WHEN THE RATIO $g_{\parallel}/g_{\perp}$ IS INCREASED WHILE ANISOTROPIC HYDROGEN AND ISOTROPIC NITROGEN COUPLING EXISTS.

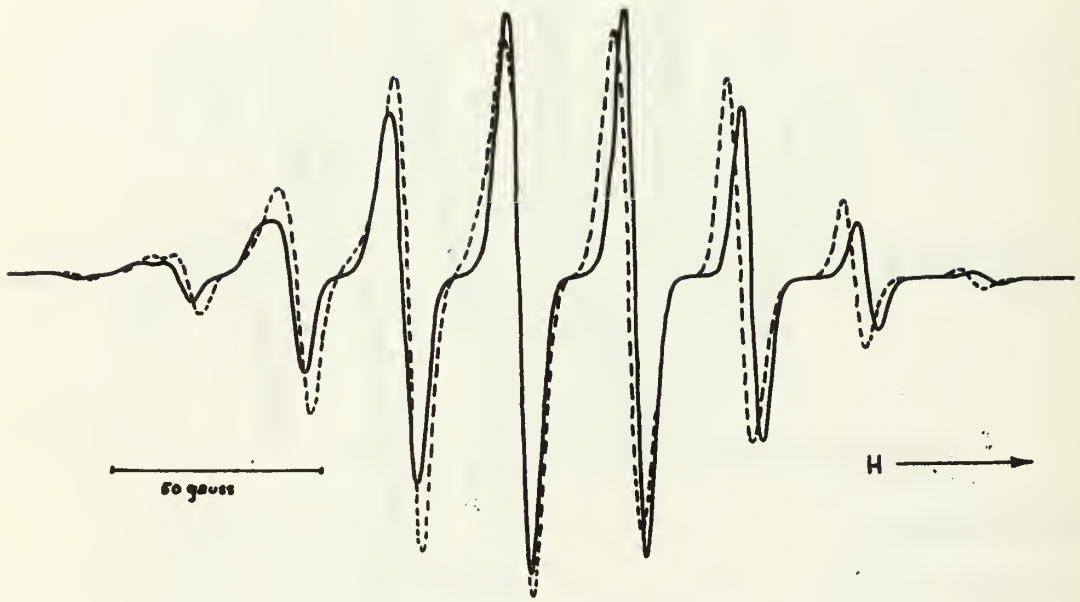

Figure 25
DIMETHYL AMIDOGEN, $(CH_3)_2N\cdot$

SOLID LINE	DASHED LINE
$A_{\parallel}^{N}$ = 27.4 G	$A_{\parallel}^{N}$ = 24.4 G
$A_{\perp}^{N}$ = 27.4 G	$A_{\perp}^{N}$ = 24.4 G
$A_{\parallel}^{H}$ = 29.4 G	$A_{\parallel}^{H}$ = 29.4 G
$A_{\perp}^{H}$ = 26.4 G	$A_{\perp}^{H}$ = 26.4 G
$g_{\parallel}$ = 2.0071	$g_{\parallel}$ = 2.0071
$g_{\perp}$ = 2.0042	$g_{\perp}$ = 2.0042

THESE CALCULATED SPECTRA INDICATE THE CHANGE WHICH OCCURS WHEN THE RATIO A^N ISOTROPIC/A^H ISOTROPIC IS INCREASED WHILE ANISOTROPIC HYDROGEN AND g COUPLING ESISTS.

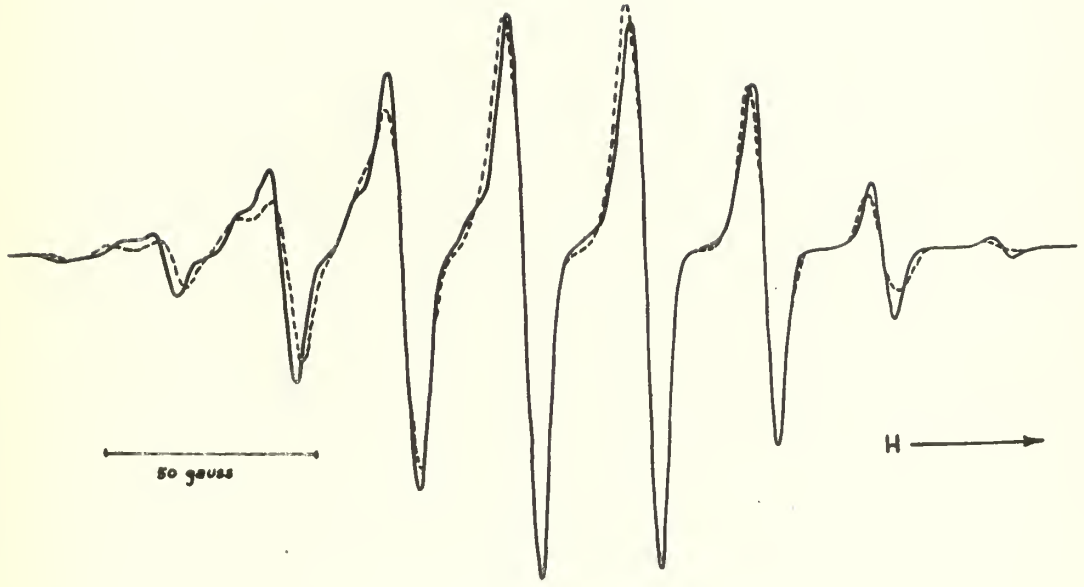

Figure 26
DIMETHYL AMIDOGEN, $(CH_3)_2N\cdot$

SOLID LINE	DASHED LINE
$A_{\parallel}^{N} = 34.2$ G	$A_{\parallel}^{N} = 34.2$ G
$A_{\perp}^{N} = 28.5$ G	$A_{\perp}^{N} = 28.5$ G
$A_{\parallel}^{H} = 27.4$ G	$A_{\parallel}^{H} = 29.4$G
$A_{\perp}^{H} = 27.4$ G	$A_{\perp}^{H} = 26.4$ G
$g_{\parallel} = 2.0071$	$g_{\parallel} = 2.0071$
$g_{\perp} = 2.0042$	$g_{\perp} = 2.0042$

THESE CALCULATED SPECTRA INDICATE THE CHANGE WHICH OCCURS WHEN THE RATIO $A_{\parallel}^{H}/A_{\perp}^{H}$ IS INCREASED WHILE ANISOTROPIC NITROGEN AND g COUPLING EXISTS.

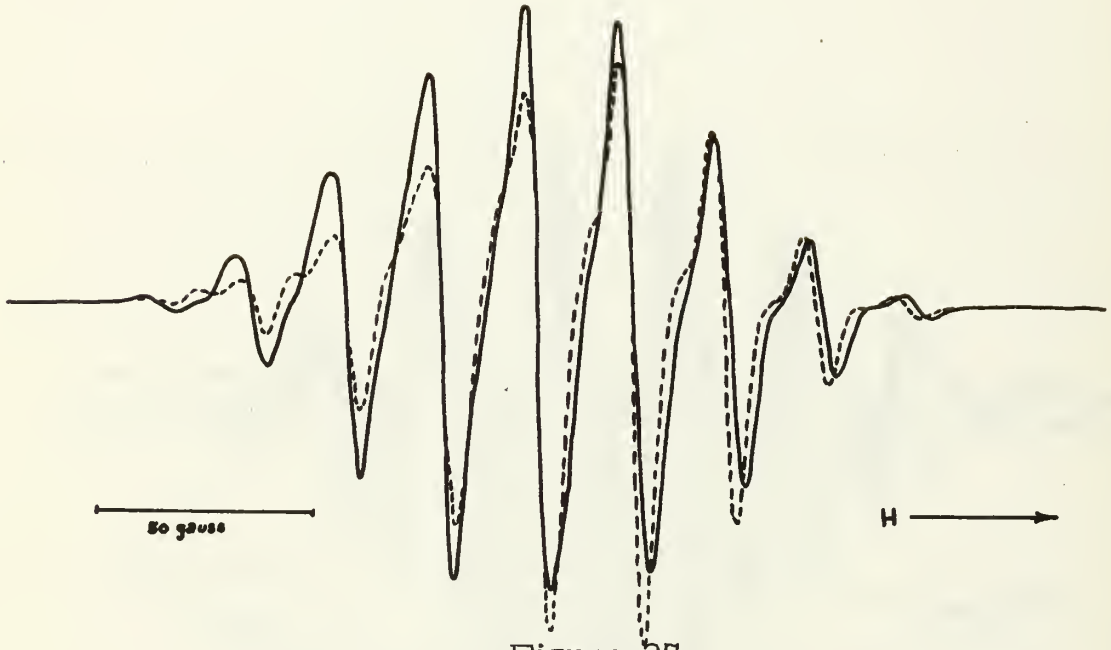

Figure 27
DIMETHYL AMIDOGEN, $(CH_3)_2N\cdot$

SOLID LINE	DASHED LINE
$A_{\parallel}^{N} = 28.2$ G	$A_{\parallel}^{N} = 28.2$ G
$A_{\perp}^{N} = 22.5$ G	$A_{\perp}^{N} = 22.5$ G
$A_{\parallel}^{H} = 20.6$ G	$A_{\parallel}^{H} = 20.6$ G
$A_{\perp}^{H} = 20.6$ G	$A_{\perp}^{H} = 20.6$ G
$g_{\parallel} = 2.0048$	$g_{\parallel} = 2.0098$
$g_{\perp} = 2.0042$	$g_{\perp} = 2.0042$

THESE CALCULATED SPECTRA INDICATE THE CHANGE WHICH OCCURS WHEN THE RATIO $g_{\parallel}/g_{\perp}$ IS INCREASED WHILE ANISOTROPIC NITROGEN AND ISOTROPIC HYDROGEN COUPLING EXISTS.

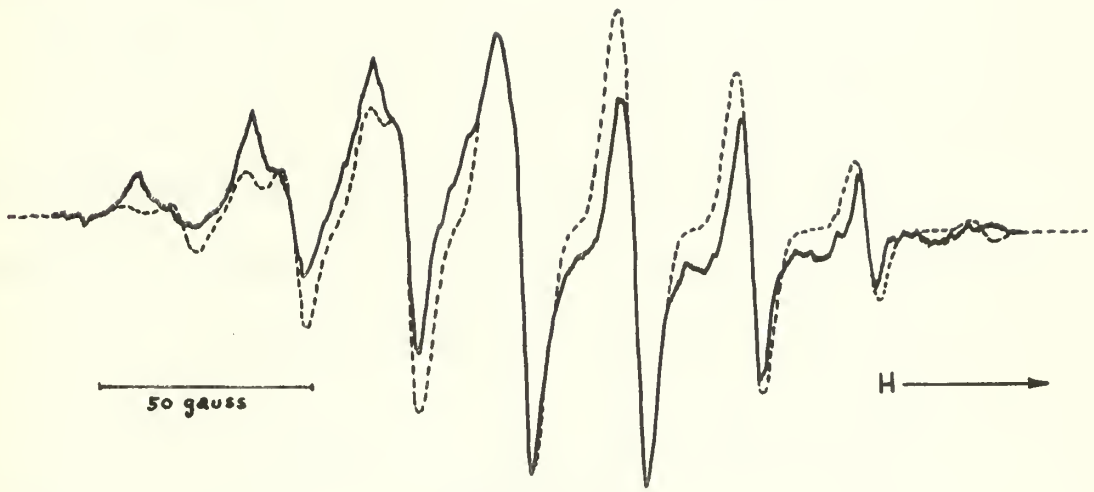

Figure 28
DIMETHYL AMIDOGEN, $(CH_3)_2N\cdot$

SOLID LINE — EXPERIMENTAL SPECTRUM

DASHED LINE

$A_{\parallel}^{N} = 27.9$ G
$A_{\perp}^{N} = 27.9$ G
$A_{\parallel}^{H} = 28.4$ G
$A_{\perp}^{H} = 25.5$ G
$g_{\parallel} = 2.0098$
$g_{\perp} = 2.0042$

THIS CALCULATED SPECTRUM REPRESENTS THE BEST CORRESPONDENCE ATTAINED WITH THE EXPERIMENTAL SPECTRUM.

9. Molecular Orbital Calculations

Hückel molecular orbital calculations were performed on the radicals dimethyl amidogen and amidogen by means of a digital computer program described as an extended Huckel theory. [16] In this calculation, by the use of an extended basis set of atomic orbitals, with the inclusion of overlap and all interactions, the Hückel theory yields a good qualitative solution of most hydrocarbon conformal problems. The calculation is applicable to aliphatic and aromatic hydrocarbon systems.

The expansion of a molecular orbital as a linear combination of atomic orbitals: $\Psi_i = \sum_j c_{ij} \Phi_j$ yields, on minimizing the total energy, the set of Huckel equations:

$$\sum_{i=1}^{n} [H_{ij} - E S_{ij}] c_{ij} = 0 \qquad j = 1, 2, 3, \cdots, n$$

The basis set of atomic orbitals consists of Hydrogen 1s, carbon 2s and 2p, and nitrogen 2s and 2p Slater atomic orbitals with the corresponding Slater exponents.

The complete secular determinant is treated, all interactions accounted for, and the off-diagonal energy terms retained. The critical choice is in the selection of these off-diagonal matrix elements. The diagonal elements, Hii are taken as valence state ionization potentials. The off-diagonal elements, Hij are taken as:

$$H_{ij} = 0.5 K (H_{ii} + H_{jj}) S_{ij} \qquad K = 1.75$$

For almost all molecules, a Hückel calculation of this

type gives rise to a potential curve having a minimum not far from the correct, experimentally determined geometry of the molecule. [16]

The parameters associated with these calculations were taken from the current literature. [38] , [39] , [45] These may be summarized as follows:

	Carbon	Nitrogen
2s valence state ionization potential	-21.4 e.v.	-27.5 e.v.
2p valence state ionization potential	-11.4 e.v.	-14.5 e.v.
Slater orbital exponent	1.625	1.950

The calculations concerned with the $\cdot NH_2$ radical were invalid. This possibility of the failure of the calculations for certain diatomic and triatomic molecules is alluded to by the originator of this calculation. [16]

The calculation seems to provide meaningful energy levels and orbitals for the $\cdot N(CH_3)_2$ radical. A series of such calculations as a function of bond angle on the nitrogen atom yields a minimum energy configuration at a bond angle of approximately 140°. The barrier related to the C-N-C bond at the 180° bond-angle position with respect to the preferred minimum energy configuration is approximately 0.5 electron volts. The existence and magnitude of this barrier has significance in the final analysis of the coupling associated with this radical. This potential energy function is indicated in Figure 29.

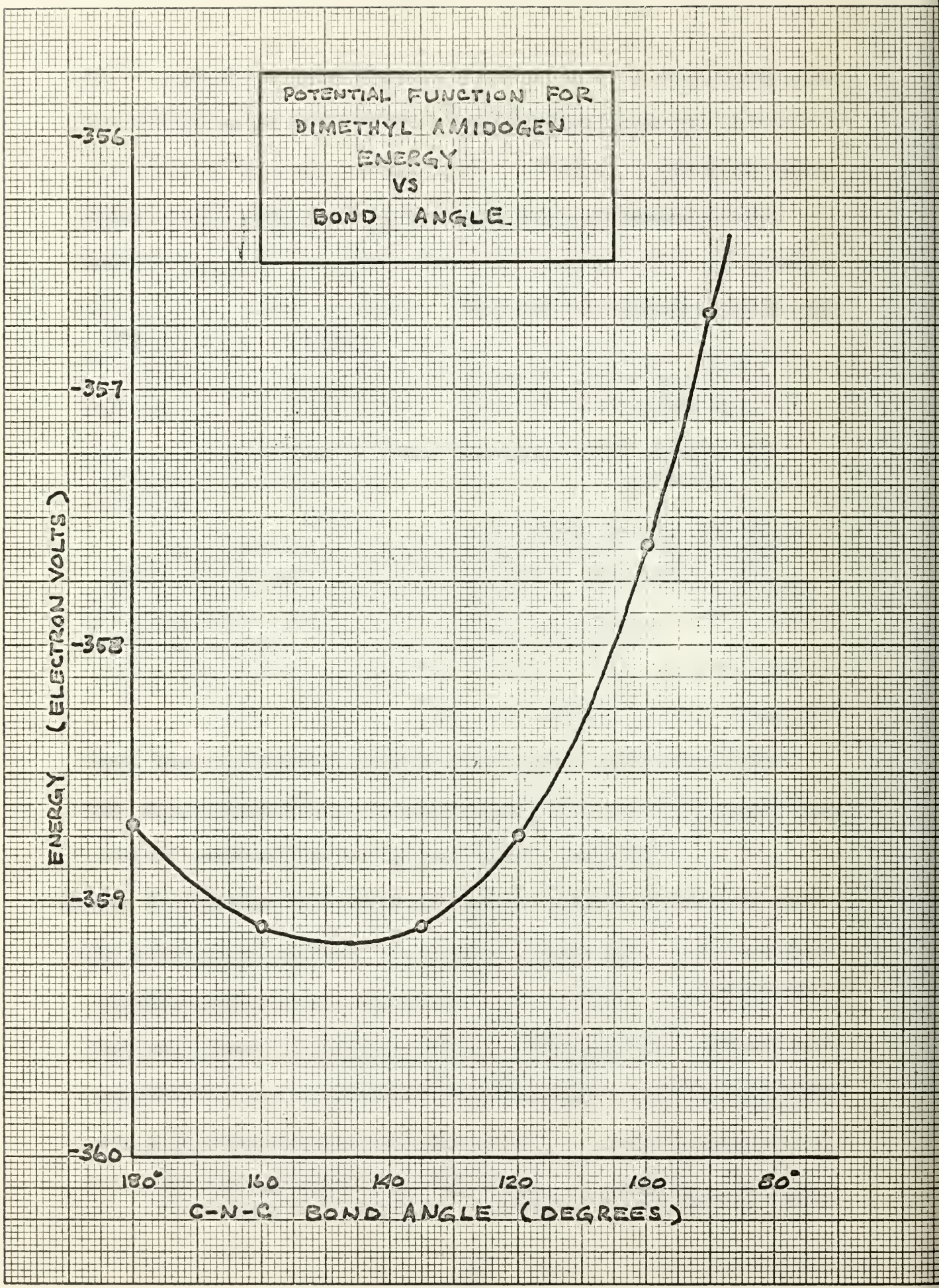
POTENTIAL FUNCTION FOR
DIMETHYL AMIDOGEN
ENERGY
VS
BOND ANGLE
-356
-357
-358
-359
-360
ENERGY (ELECTRON VOLTS)
180°
160
140
120
100
80°
C-N-C BOND ANGLE (DEGREES)

Figure 29

The calculated coefficients of the atomic orbitals which comprise the molecular orbital indicate that the unpaired electron is largely localized to the nitrogen p-orbital, perpendicular to the plane formed by the bent structure of the molecule. A diagrammatic representation of the radical is given by Figure 30.

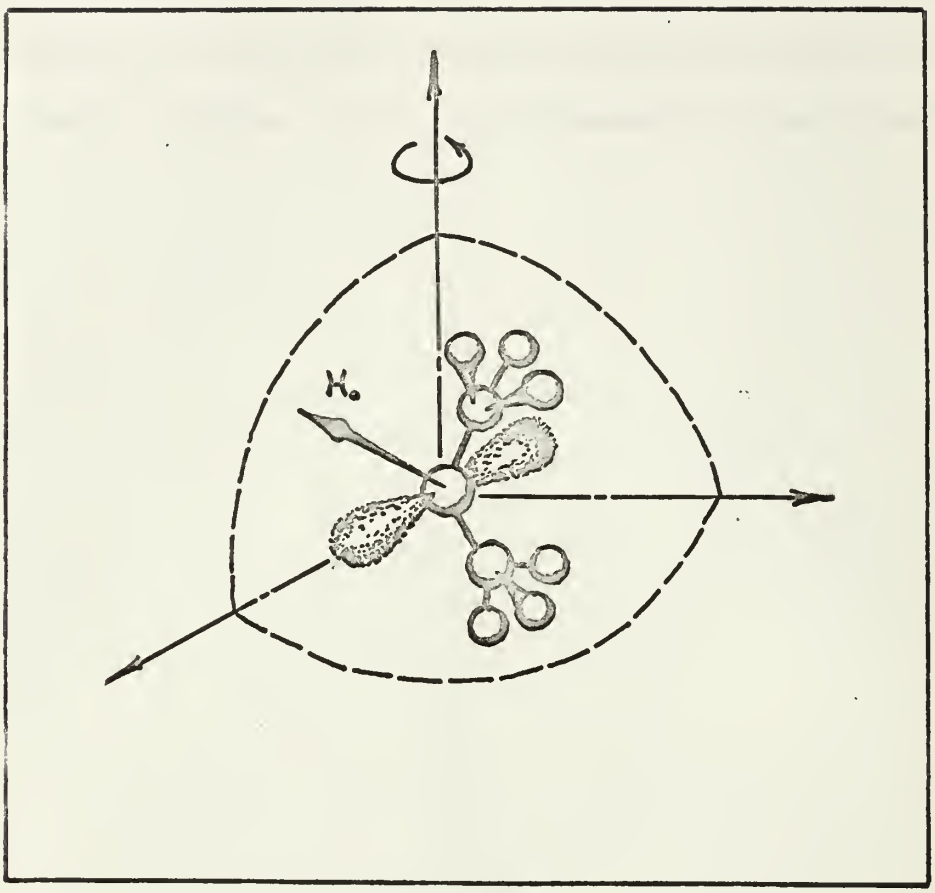

Figure 30

Diagrammatic Representation of Dimehyl Amidogen

10. Conclusions

One of the principal reasons for selection of the radical species dimethyl amidogen as the subject of this investigation was due to the speculation regarding its existence and its relationship to other simple nitrogen-containing radicals which have recently been reported. This relationship may be represented diagrammatically as follows:

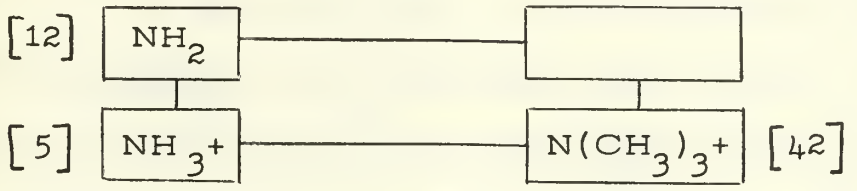

The first of this series to be investigated was the radical NH_2 in 1958. The radical was formed by electrical discharge from ammonia in an argon matrix. The spectrum indicates an almost total free, random rotation of the radical at liquid helium temperatures. [12]

The second of this series to be investigated was the radical NH_3^+ in 1961. The radical was formed by the X-ray irradiation from a single crystal of ammonium perchlorate. The spectrum indicates typical anisotropic tensor orientation dependence. [5]

The third of this series to be investigated was the radical $N(CH_3)_3^+$ in 1962. The radical was formed by γ-ray irradiation from a single crystal of tetramethyl ammonium chloride. The spectrum indicates an axially-symmetric anisotropic tensor orientation dependence. [42]

The identification and characterization of dimethyl amidogen would, so-to-speak, complete the loop of the series shown.

Earlier workers [36],[40],[15] have obtained evidence as to the existence of a radical species formed by the photolysis of tetramethyl tetrazene as follows:

$$(CH_3)_2\text{-N-N=N-N-}(CH_3)_2 \xrightarrow{h\nu} 2\,(CH_3)_2N\cdot + N_2$$

Other sources of this radical are indicated to be: [13]

$$(CH_3)_2NH + h\nu \longrightarrow (CH_3)_2N + H$$

$$(CH_3)_3N + h\nu \longrightarrow (CH_3)_2N + CH_3$$

$$(CH_3)_2N\text{-NO} + h\nu \longrightarrow (CH_3)_2N + NO$$

$$(CH_3)_2NCl + Cu \longrightarrow (CH_3)_2N + CuCl$$

Despite these indicated sources of the radical, no definitive work has been published on this radical.

As a first step in the correlation of the results of this investigation of dimethyl amidogen with the previous work concerning the other radical species in the series, a comparison of the isotropic tensor components would likely have the largest validity. This is due in part to the degree of the fit of the computed spectra to the experimental spectra and in part to the apparent molecular rotation which appears to be characteristic of the series.

	NH_2	NH_3^+	$N(CH_3)_3^+$	$N(CH_2)_2$
A^N	10.3 G	19.5 G	18.0 G	27.9 G
A^H	23.9 G	25.9 G	26.7 G	26.4 G

The coupling associated with the methyl group equivalent

protons appears to correlate satisfactorily, whereas that associated with the nitrogen is appreciably larger than the others in this series. An explanation of this seeming discrepancy may be found in an alysis of the nitrogen coupling as a function of bond angle. This analysis has been completed for the $\cdot NH_2$ radical with a SCF-LCAO-MO theory which has also been applied to the $\cdot CH_3$ radical. [15] The nitrogen coupling for $\cdot NH_2$ corresponding to an experimentally determined bond angle of 103° was calculated to be 14.7 G. This corresponds satisfactorily with the experimental nitrogen coupling of 10.3 G. As the bond angle is increased the coupling associated with the nitrogen atom also increases. For example, at 120° the calculated coupling for nitrogen was determined to be 19.0 G, and at 140° the calculated coupling was determined to be 27.5 G.

If, as an approximation, the calculated coupling for nitrogen in the $\cdot NH_2$ radical were applied to all the radicals in this series the correlation between nitrogen coupling and bond angle becomes satisfactory.

Both of the radicals NH_3^+ and $N(CH_3)_3^+$ are planar or nearly so. [5], [42] The bond angle is therefore 120° and the experimental couplings of 19.5 G and 18.0 G correlate well with the calculated 19.0 G at that bond angle.

The Huckel M.O. calculations for $N(CH_3)_2$ indicate that the bond angle is approximately 140°. The calculated coupling of 27.5 G correlates well with the experimental 27.9 G.

In considering next the anisotropic component of the proton coupling tensors, the calculated spectra indicate that such anisotropies are no greater than the 3.0 G reported for the best fit. Larger anisotropies lead to a considerable broadening of the higher field lines contrary to experimental evidence. These results are consistent with those reported for the $(CH_3)_2CCOOH$ radical.[17] The anisotropy reported was 2.2 G with the parallel component greater than the perpendicular component, and a compilation of other similar radicals yielded a total spread of only 2.5 G as the range of anisotropies for such species. One consequence of this narrow range is that a rotating methyl group next to a radical center should always give a clear pattern of fairly narrow lines even in polycrystalline solids.

The final aspect in the correlation of this investigation is that related to the anisotropy, or lack of anisotropy, in the nitrogen coupling. The interaction between the unpaired electron in a p-orbital of an atom and the magnetic nucleus of that atom is usually found to be an axially symmetric tensor.[30] From the Hückel M.O. calculations this is the situation for dimethyl amidogen, as it is with all the other members of the series. In the series, NH_3^+ and $N(CH_3)_3^+$ have anisotropic components of the nitrogen coupling which have been resolved. However, in both the these radicals there was some degree of rotation of the molecule assumed in an attempt

to explain the spectra. The spectrum of NH_2 is indicative of almost total random rotation of the molecule even at liquid helium temperatures.

Therefore, even considering the degree of the best fit of the calculated $N(CH_3)_2$ spectra with respect to the experimental, there is undoubtedly some degree of molecular rotation involved. This molecular rotation must be assumed to offer an explanation for the isotropic nitrogen coupling which is reported as the result of this investigation.

Taken as a complete set, the correlations between the results of this investigation and the other radicals in the series appear to be satisfactory.

This investigation has then established the identification of the dimethyl amidogen radical and furthermore that the radical is indeed the photolytic decomposition product of tetramethyl tetrazene. It might also be noted that if the radical could be produced from the photolysis of dimethyl amine as indicated, it was not observed in this investigation and would seem to require a more energetic source of irradiation than used here. Also the decomposition of dimethyl amine with a tesla coil did not produce the dimethyl amidogen radical, but instead, some other unidentified paramagnetic species.

It might be appropriate at this point to consider the proposal[2],[32] that an ordinary tesla coil provides a convenient laboratory tool for producing free radicals in the con-

densed phase. A fairly large number of molecules were subjected to this technique in the course of this investigation. It must be noted that in every case a paramagnetic species was indeed produced. The identification and analysis of these spectra was in general not attempted due to the lack of resolved hyperfine structure. One additional complicating factor was the presence or suspected presence of more than one paramagnetic species. This latter complication might be resolved by the use of a variable temperature system which would allow the experimentalist to remove all but one species.

In general, however, the procedure seems to merit further investigation in view of the fact that paramagnetic species are produced, whereas, ultraviolet irradiation did not produce radicals with the same substrate in most instances. The tesla coil is certainly a more convenient energy source than X-ray or γ-Ray sources.

Finally, an evaluation of the general procedure used to interpret polycrystalline spectra should close this report. The results of this investigation seem to indicate the feasibility of the project in general terms. However, the procedure in practical terms is too lengthy and time consuming in the existing form for anything but the simpler radicals. With no supporting data as to the isotropic components of the tensors, the trial and error process is prohibitive.

It may prove to be possible to perform the iterative

solution in the digital computer program with some incorporated least-squaring routine, but not without some drastic reduction in the current computer time required with the existing program.

11. Bibliography

1. Abragam, A., Pryce, M. H. L., Proceedings Royal Society (London), A205, 135 (1951).

2. Bass, A. M., Broida, H. P., Formation and Trapping of Free Radicals, Academic Press (1960).

3. Blinder, S. M., Journal of Chemical Physics, 33, 748 (1960).

4. Bull, W.E., Seaton, J.A., Audrieth, L. F., Journal of American Chemical Society, 80, 2516 (1957).

5. Cole, T., Journal of Chemical Physics, 35, 1169 (1961).

6. Cole, T., Pritchard, H., Davidson, N., McConnell, H., Molecular Physics, 1, 406 (1958).

7. Das, M. R., Patankar, A. V., Venkataraman, B., Proceedings of the Indian Academy of Sciences, 53A, (1961).

8. Dixon, W. T., Norman, R. O. C., Journal of Chemical Society, 3119 (1963).

9. Dixon, W. T., Norman, R.O. C., Journal of Chemical Society, 3625 (1964).

10. Dixon, W. T., Norman, R. O. C., Journal of Chemical Society, 4850 (1964).

11. Dixon, W. T., Norman, R. O. C., Journal of Chemical Society, 4857 (1964).

12. Foner, S. N., Cochran, E. L., Bowers, V. A., Jen, C. K., Physical Review Letters, 1, 91 (1958).

13. Gould, R. F., Advances in Chemistry Series, American Chemical Society (1962).

14. Heller, C., McConnell, H. M., Journal of Chemical Physics, 32, 1535 (1960).

15. Higuchi, J., Journal of Chemical Physics, 35, 2270 (1961).

16. Hoffman, R., Journal of Chemical Physics, 39, 1397 (1963).

17. Horsfield, A., Morton, J. R., Whiffen, D. H., Transactions Faraday Society, 57, 1657 (1961).

18. Horsfield, A., Morton, J. R., Whiffen, D. H., Molecular Physics, 4, 327 (1961)

19. Kasai, P. H., Kirshenbaum, A. D., Journal of the American Chemical Society, 87, 3069 (1965)

20. Kholmogorov, V. E., Baranov, E. V., Optics and Spectroscopy, 14, 440 (1963)

21. Kneubuhl, F. K., Journal of Chemical Physics, 33, 1074 (1960).

22. Kohin, R. P., Nadeau, P. G., Journal of Chemical Physics, 44, 691 (1966)

23. Lefebvre, R., Journal of Chemical Physics, 33, 1826 (1960).

24. Lefebvre, R., Maruani, J., Journal of Chemical Physics, 42, 1480 (1965).

25. Lin, W. C., McDowell, C.A., Molecular Physics, 4, 333 (1961).

26. Lin, W. C., McDowell, C.A., Molecular Physics, 4, 343 (1961).

27. Luck, C. F., Gordy, W., Journal of American Chemical Society, 78, 3240 (1956).

28. Malley, M. M., Journal of Molecular Spectroscopy, 17, 210 (1965).

29. McConnell, H. M., Heller, C., Cole, T., Fessenden, R. W., Journal of American Chemical Society, 82, 766 (1960).

30. Morton, J. R., Chemical Reviews, 453, August (1964).

31. Pake, G. E., Paramagnetic Resonance, W.A. Benjamin, Inc., (1962).

32. Papazian, H. A., Journal of Chemical Physics, 27, 813, (1957).

33. Pierson, R. H., Fletcher, A. N., Gantz, E.S., Analytical Chemistry, 28, 1237 (1956).

34. Pooley, D., Whiffen, D. H., Molecular Physics, 4, 81 (1961).

35. Renouf, E., BER 13, 2173 (1880).

36. Rice, R. O., Grelecki, C., Journal of the American Chemical Society, 79, 2679 (1957)

37. Rowlands, J. R., Whiffen, D. H., Molecular Physics, 4, 349 (1961).

38. Skinner, H. A., Pritchard, H. O., Transactions of Faraday Society, 49, 1254 (1953).

39. Skinner, H. A., Pritchard, H. O., Chemical Reviews, 55, 745 (1955).

40. Sowden, R. G., Davidson, N., Journal of the American Chemical Society, 78, 1291 (1956).

41. Sternlicht, H., Journal of Chemical Physics, 33, 1128 (1960).

42. Tench, A. J., Journal of Chemical Physics, 38, 593 (1963).

43. Tench, A. J., Journal of Physical Chemistry, 67, 923 (1963).

44. Tolles, W. M., To be published, Journal of American Chemical Society, (1966).

45. Wiberg, K. B., Physical Organic Chemistry, John Wiley & Sons (1964).

APPENDIX I

TETRAMETHYL - 2 - TETRAZENE

When this study was commenced, the tetramethyl-2-tetrazene used was from a sample obtained from the Research Department of the U. S. Naval Ordnance Test Station, China Lake, California, for another study [44] on the cation radical of that molecule.

A radical species was produced from this sample by the methods described elsewhere in this paper, but seemingly there was more than the single, desired radical species being produced. Furthermore, on successive attempts the apparent concentration of the species varied markedly.

It was considered likely that a contaminant or decomposition product was present in the tetramethyl-2-tetrazene and subsequently a fresh quantity was produced as described elsewhere in this paper.

The infrared spectrum of the locally produced tetramethyl-2-tetrazene was obtained with a Perkin Elmer 337 Grating Spectrometer and compared exactly with the published spectrum. [33] Figures 31 and 32 comprise the entire spectrum taken with a 10 cm. path-length gas cell at a pressure of 8 mm. at room temperature.

In a further attempt to ascertain the degree of purity of the tetramethyl-2-tetrazene, a gas chromatogram was obtained with the Beckman GC-4 Gas Chromatograph. Fig-

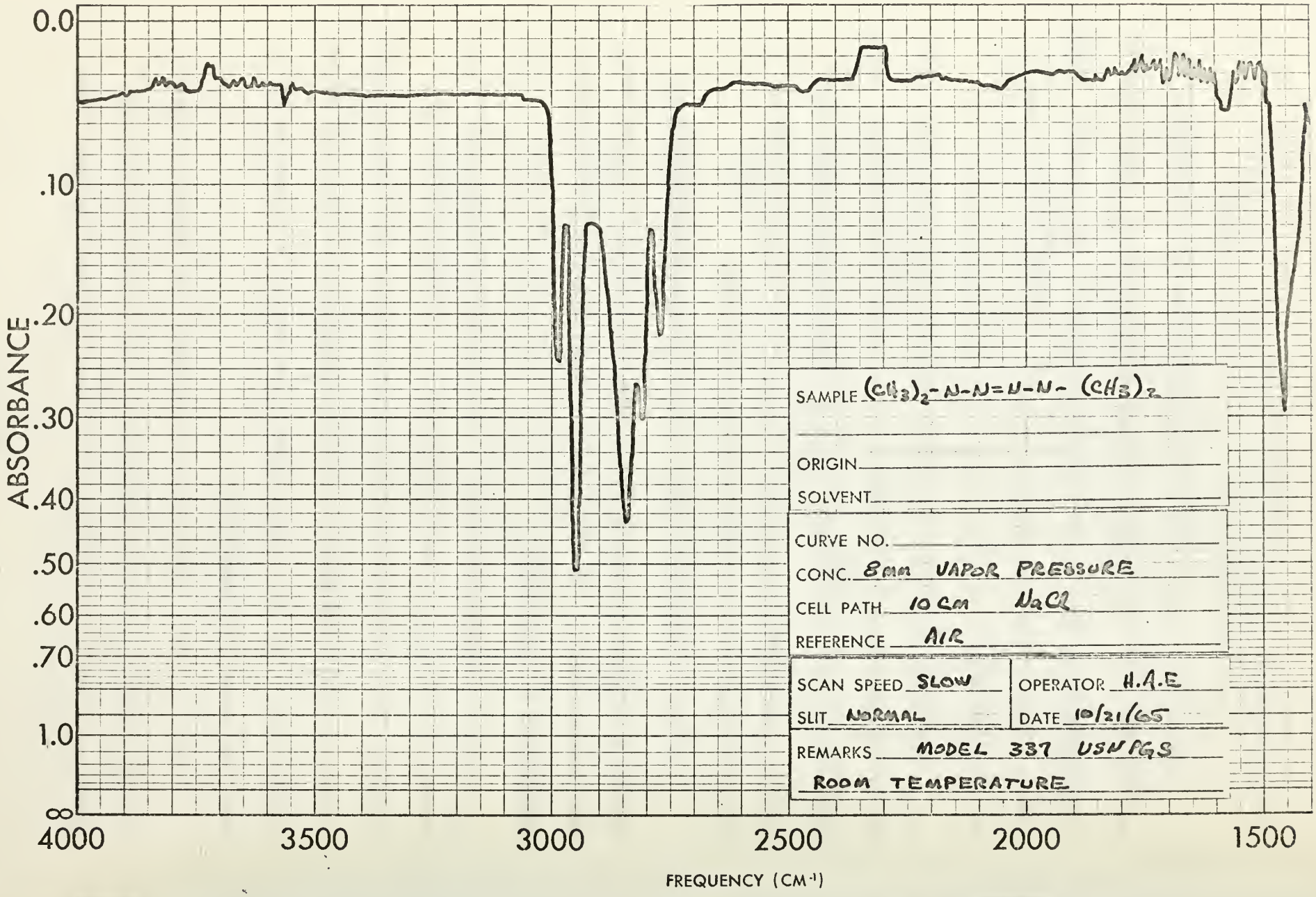
0.0
.10
.20
.30
.40
.50
.60
.70
1.0
∞
ABSORBANCE
4000
3500
3000
2500
2000
1500
FREQUENCY (CM⁻¹)
SAMPLE (CH3)2-N-N=N-N-(CH3)2
ORIGIN
SOLVENT
CURVE NO.
CONC. 8mm VAPOR PRESSURE
CELL PATH 10 Cm NaCl
REFERENCE AIR
SCAN SPEED SLOW
SLIT NORMAL
OPERATOR H.A.E
DATE 10/21/65
REMARKS MODEL 337 USNPGS
ROOM TEMPERATURE

Figure 31

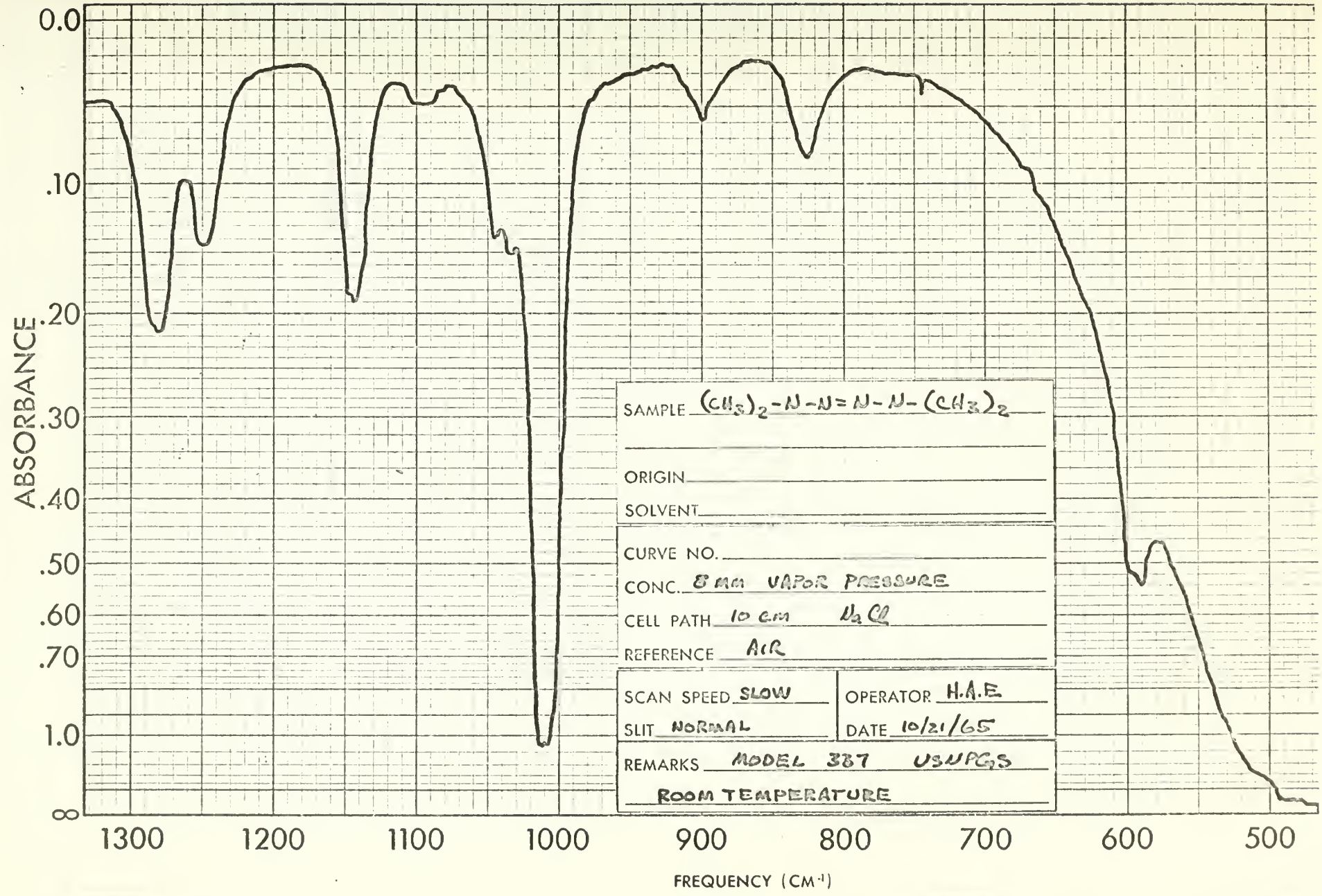
0.0
.10
.20
.30
.40
.50
.60
.70
1.0
ABSORBANCE
1300
1200
1100
1000
900
800
700
600
500
FREQUENCY (CM⁻¹)
SAMPLE (CH3)2-N-N=N-N-(CH3)2
ORIGIN
SOLVENT
CURVE NO.
CONC. 8 MM VAPOR PRESSURE
CELL PATH 10 cm NaCl
REFERENCE AIR
SCAN SPEED SLOW
SLIT NORMAL
OPERATOR H.A.E
DATE 10/21/65
REMARKS MODEL 337 USNPGS
ROOM TEMPERATURE

Figure 32

ure 33 is the representation obtained with a 100°C isothermal run. Discounting the first air peak, the area of the four small peaks given by the recording integrator is 4.2. The area of the main tetramethyl-2-tetrazene is 238.5. The uncorrected apparent degree of impurity is then 1.8%. However, the height of the four minor peaks is strongly temperature-dependent, indicating that they are likely decomposition products and therefore the degree of impurity is somewhat less than 1.8%.

In any event, this quantity of tetramethyl-2-tetrazene was used to produce the radical species dimethyl amidogen. The spectrums of the radical appeared to be without a second species and totally reproducible.

The tetramethyl-2-tetrazene used in the formation of the dimethyl amidogen radical was prepared according to the basic scheme of the Renouf Method[35] as modified by subsequent workers.[4]

The scheme is basically the oxidation of 1,1 dimethyl hydrazine with mercuric oxide.

$$2(CH_3)_2\text{-N-N-(H)}_2 \longrightarrow (CH_3)_2\text{-N-N=N-N-}(CH_3)_2$$

One mole (60.1 g.) of 1,1 dimethyl hydrazine obtained from Eastman Chemicals was diluted with 375 ml. ether in a 2 l. three-necked flask, fitted with a mechanical stirrer and reflux condenser. The flask was immersed in an ice bath and the yellow mercuric oxide was added slowly through the reflux

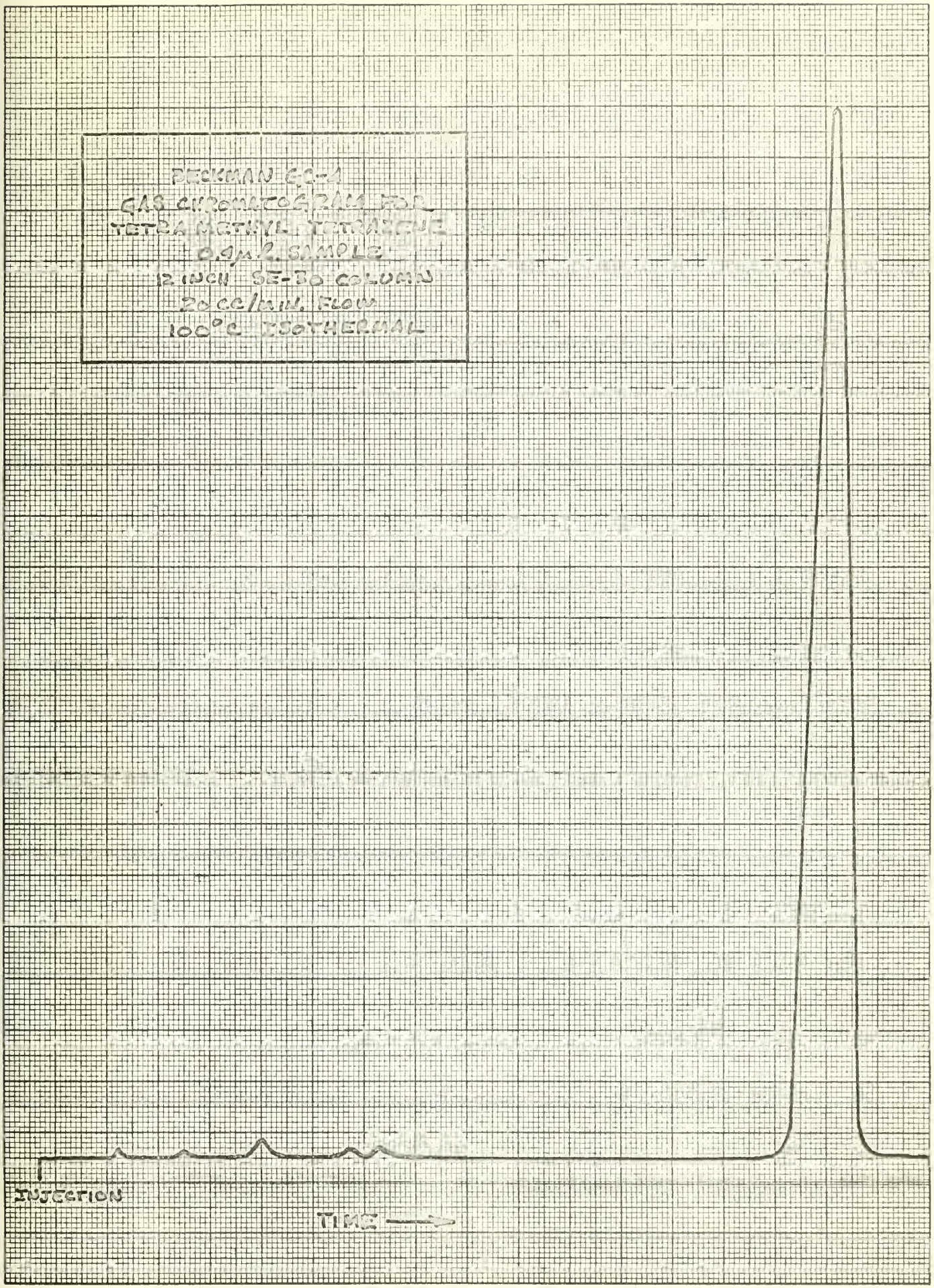
PECKMAN GC-1
GAS CHROMATOGRAM FOR
TETRA METHYL TIN IN
0.4 µL SAMPLE
12 INCH SE-30 COLUMN
20 CC/MIN. FLOW
100°C ISOTHERMAL
INJECTION
TIME

Figure 33

condenser over a period of one hour.

After 45 minutes and the addition of 185 g.HgO the reaction mixture cleared. Subsequent quantities of the mercuric oxide reacted almost instantly. A total of one mole (216.6 g.) of HgO was added, the reaction mixture reverting to a yellow color during the last stages of the addition.

Another two hours were allowed for the reaction to proceed to completion, at which time the reaction mixture was filtered to remove the unreacted mercuric oxide and the free mercury.

The ethereal solution was separated from the aqueous layer which formed during the course of the reaction, and the water layer was extracted with ether. The combined ether solutions were then dried with anhydrous sodium sulfate.

The dried ether solution was then concentrated with a rotary evaporator until there appeared to be no further evaporation of ether. The remaining solution was distilled at reduced pressure (9.5 - 10.0 cm. Hg) and, the fraction within the boiling range 72 - 75°C was collected. This fraction was purified by redistillation at reduced pressure (9.5 - 10.0 cm. Hg) from fused barium axide. The fraction with the boiling range 72 - 75°C was collected again.

A yield of 38.6 g. was obtained corresponding to a 66.4% yield. The boiling point of the purified tetramethyl-2-tetrazene so obtained was determined to be 124°C at a local atmospheric

pressure of 765.2 mm. Hg.

A plot of vapor pressure as a function of reciprocal temperature is shown on Figure 34. The literature values[4] plot as a relatively straight line. Also shown is the boiling range of the prepared tetramethyl-2-tetrazene, which is in agreement with the accepted values. The boiling point at atmospheric pressure is somewhat lower (124°C) compared to that reported (134°C).

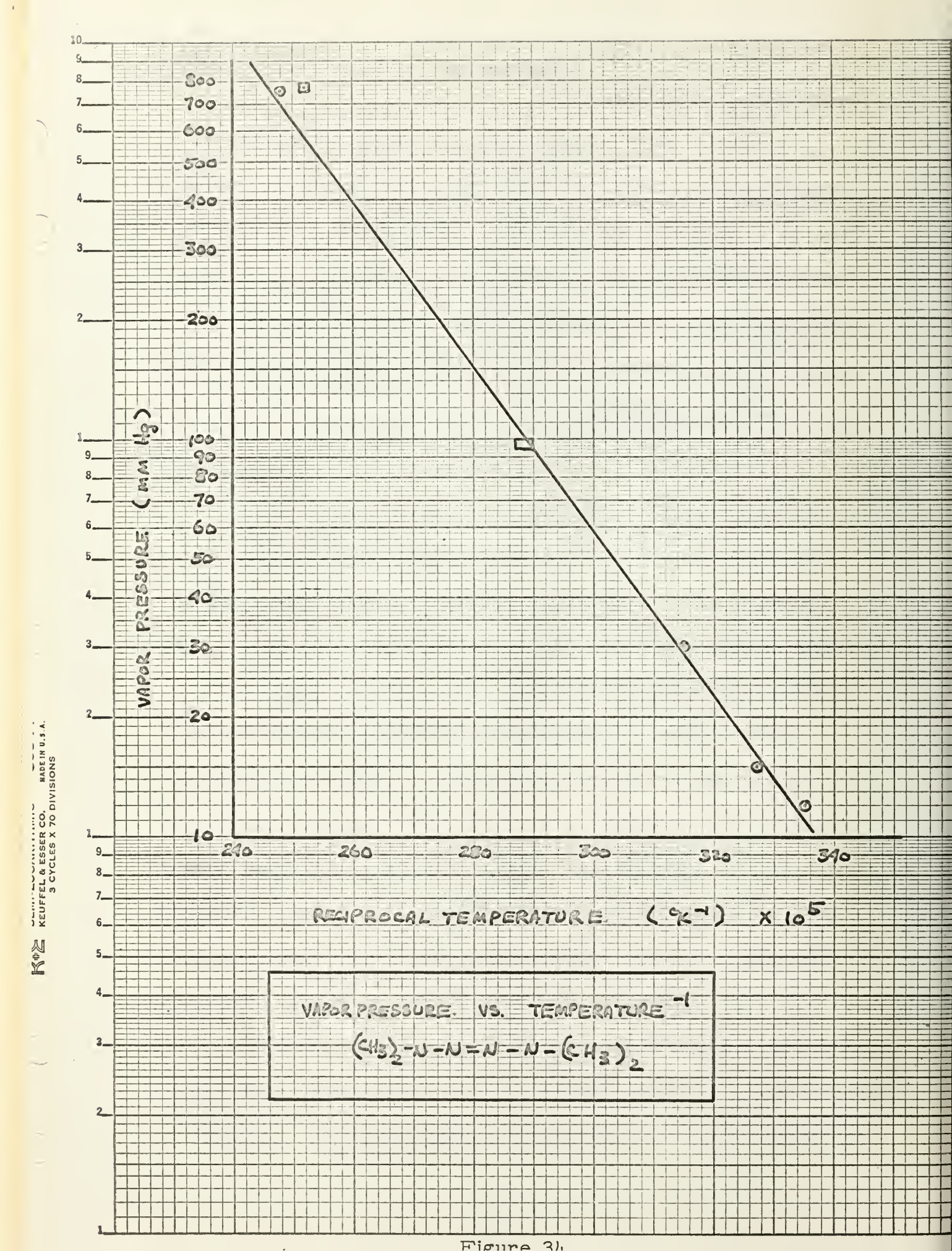
VAPOR PRESSURE (mm Hg)
800
700
600
500
400
300
200
100
90
80
70
60
50
40
30
20
10
240
260
280
300
320
340
RECIPROCAL TEMPERATURE (°K⁻¹) X 10⁵
VAPOR PRESSURE VS. TEMPERATURE⁻¹
(CH3)2-N-N=N-N-(CH3)2
KEUFFEL & ESSER CO. MADE IN U.S.A.
3 CYCLES X 70 DIVISIONS

Figure 34

APPENDIX II

LORENTZIAN LINE SHAPES

In any E.P.R. spectroscopy experiment the worker must guard against what is termed "modulation broadening" of the resonance line shapes. These line shapes are, in general, either Lorentzian or Gaussian in nature, the Lorentzian shapes being associated with liquid-phase spectra and the Gaussian shapes with solid-phase spectra.

It is when the radical is being observed in the liquid phase that the narrower lines are observed and, therefore, the situation in which modulation broadening is most critical. For that reason an analysis of the degree of broadening was performed on the radical formed from sodium and ammonia. The spectrum consists of a singlet with an extremely small line width.

Figures 35 and 36 show the effect of increasing modulation amplitude on the singlet spectrum. To generalize on the results of this investigation, the results can be expressed as ratios of observed values to actual values.

The Lorentzian line shape $f(\omega)$ may be expressed as a function of frequency ω, an amplitude parameter A, a width parameter T_2, and the center frequency ω_o;

$$f(\omega) = \frac{A}{1 + T_2^2(\omega - \omega_o)^2}$$

The derivative of this line shape is what is generally displayed as an E.P.R. spectrum; consequently, taking the

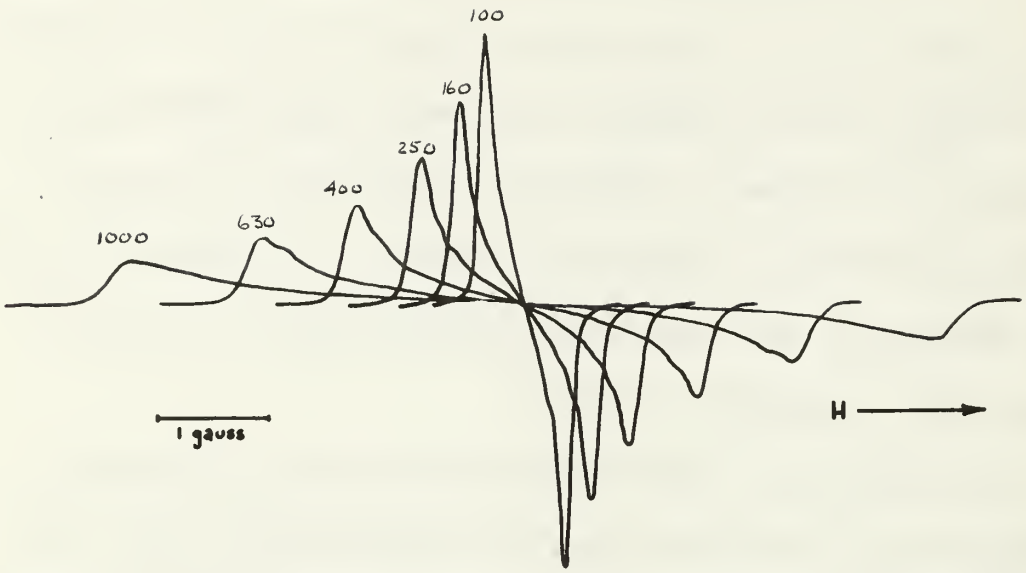

Figure 36 - Effect of Modulation Amplitude (High Range) on Radical Species N_a in NH_3

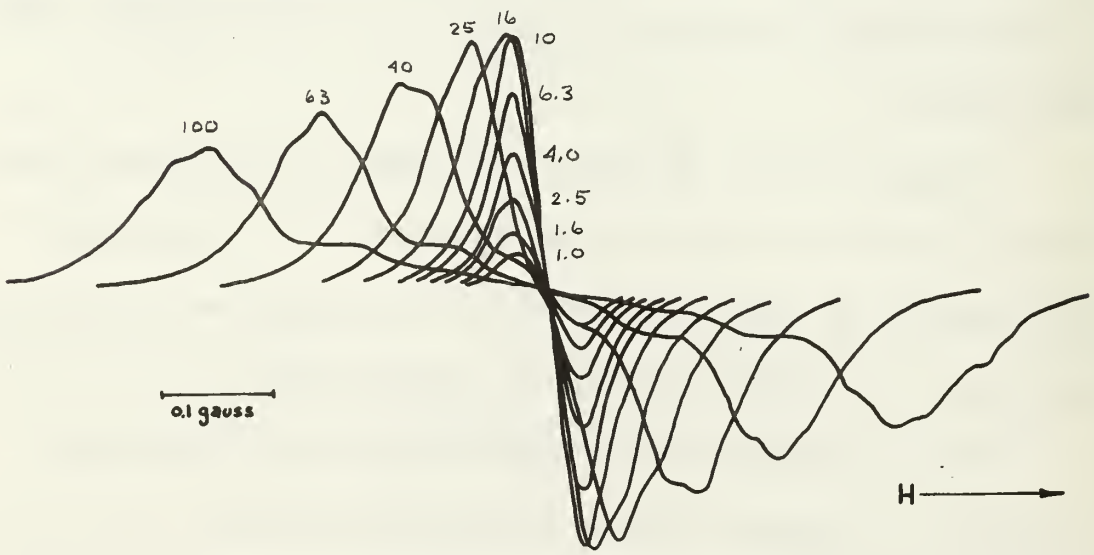

Figure 35 - Effect of Modulation Amplitude (Low Range) in Radical Species N_a in NH_3

derivative, one obtains:

$$f'(\omega) = - \frac{2AT_2^2(\omega-\omega_o)}{[1+T_2^2(\omega-\omega_o)^2]^2}$$

To obtain the line width of this derivative spectrum one must determine the frequencies of the extrema by taking the second derivative of the above expression;

$$f''(\omega) = \frac{6AT_2^4(\omega-\omega_o)^2 - 2AT_2^2}{[1+T_2^2(\omega-\omega_o)^2]^3}$$

Then the location of the extrema are given by:

$$\omega-\omega_o = \pm \frac{1}{\sqrt{3}T_2}$$

Let the peak-to-peak line width of the derivative of the Lorentzian line shape be W.

$$W = \frac{2}{\sqrt{3}T_2}$$

Now evaluate the expression, $f'(\omega)$, at $\omega-\omega_o = \pm \frac{1}{\sqrt{3}T_2}$ to obtain the peak-to-peak height of the derivative of the Lorentzian line shape.

$$f'(\omega_o \pm \frac{1}{\sqrt{3}T_2}) = - \frac{9AT_2}{8\sqrt{3}} = - \frac{6A}{8W}$$

As these peaks are symmetric, we can define the peak-to-peak height as P.

$$P = \frac{9AT_2}{4\sqrt{3}} = \frac{6A}{4W}$$

The approximation to the derivative of the Lorentzian line shape, $f'_{app}(\omega)$ or that line shape which is actually observed due to the modulation, is expressed in terms of the same parameters as used previously with the inclusion of the modulation amplitude, m.

$$f'_{app}(\omega) = \frac{A}{[1+T_2^2(\omega+\frac{m}{2}-\omega_o)^2]} - \frac{A}{[1+T_2^2(\omega-\frac{m}{2}-\omega_o)^2]}$$

Proceeding as before, the frequencies of the extrema may be

determined from the second derivative.

$$f''_{app}(\omega) = -\frac{2AT_2^2(\omega+\frac{m}{2}-\omega_0)}{\left[1+T_2^2(\omega+\frac{m}{2}-\omega_0)^2\right]^2} + \frac{2AT_2^2(\omega-\frac{m}{2}-\omega_0)}{\left[1+T_2^2(\omega-\frac{m}{2}-\omega_0)^2\right]^2}$$

Then the location of the extrema are given by:

$$\omega-\omega_0 = \pm\left[\frac{m^2T_2^2-4+2\sqrt{m^4T_2^4+4m^2T_2^2+16}}{12T_2^2}\right]^{\frac{1}{2}}$$

And the peak-to-peak line width of the approximation to the derivative of the Lorentzian line shape is given by:

$$W_{app} = 2\left[\frac{m^2T_2^2-4+2\sqrt{m^4T_2^4+4m^2T_2^2+16}}{12T_2^2}\right]^{\frac{1}{2}}$$

The expression for $f'_{app}(\omega)$ can be evaluated at the frequency corresponding to the extrema.

$$f'_{app}(\omega) = -\frac{(144)(2AT_2^2m)\left[\frac{m^2T_2^2-4+2\sqrt{m^4T_2^4+4m^2T_2^2+16}}{12T_2^2}\right]^{\frac{1}{2}}}{8m^4T_2^4+128m^2T_2^2+128+(32-8m^2T_2^2)\sqrt{m^4T_2^4+4m^2T_2^2+16}}$$

As these peaks are also symmetric, the peak-to-peak height of the approximation to the derivative of the Lorentzian line shape is:

$$P_{app} = \frac{\frac{288}{\sqrt{3}}AmT_2\left[m^2T_2^2-4+2\sqrt{m^4T_2^4+4m^2T_2^2+16}\right]^{\frac{1}{2}}}{8m^4T_2^4+128m^2T_2^2+128+(32-8m^2T_2^2)\sqrt{m^4T_2^4+4m^2T_2^2+16}}$$

With these expressions, it is now possible to calculate the effect of the modulation amplitude on the Lorentzian line shape and then compare the theoretical results with what can be observed in actuality.

Consider first the effect on the line width. The expression giving the ratio of the observed line width to the true line width is:

$$\frac{W_{app}}{W} = \frac{\left[m^2T_2^2-4+2\sqrt{m^4T_2^4+4m^2T_2^2+16}\right]^{\frac{1}{2}}}{2}$$

Without loss in generality, mT_2 may be regarded as the independent variable used to compute this ratio, since mT_2

is related to $\frac{m}{W}$ which is the desired independent variable.

$$\frac{m}{W} = \frac{\sqrt{3}}{2} m T_2$$

This expression is solved for various values of the product mT_2, and the ratio of observed-line-width to true-line-width is plotted as a function of the ratio of modulation amplitude to the true-line-width.

The experimental counterpart of this curve can be determined from the experimental spectra shown in Figure 35 and 36. It is noted that the observed-line-width approaches the true-line-width as the modulation amplitude approaches zero. Therefore, the line width observed corresponding to the smallest modulation amplitude is assumed to be the true-line-width. The ratio of line widths corresponding to higher values of modulation amplitude can be taken with respect to this "near" true line width. The modulation amplitudes correspond to dial settings on the particular apparatus, but can be converted to modulation amplitudes in Gauss by the conversion procedure indicated elsewhere in the report. Thus the ratio of modulation amplitude to the true line width can be formed.

These two curves of the theoretical and experimental analysis of line broadening are shown in Figure 37 and appear to be coincident.

Proceeding to the effect of modulation on peak-to-peak height, one is unable to formulate an expression for the ratio

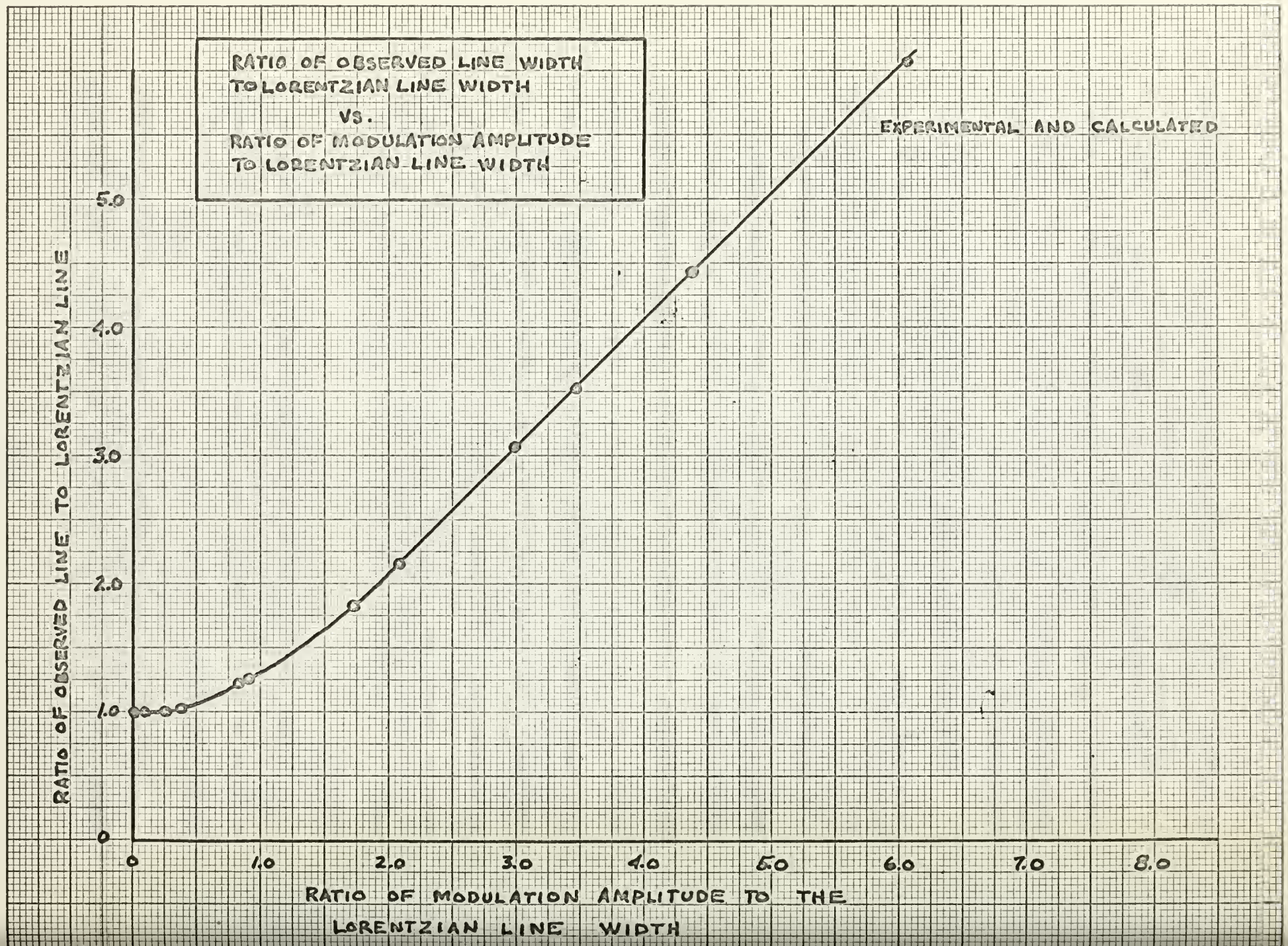

Figure 37

of observed values to actual values which has meaning. The expression for the approximate derivative line shape is not mathematically consistent with the expression for the actual derivative line shape insofar as the amplitudes are concerned.

However, the experimentalist is not directly concerned with a ratio as such. What is needed is the trade-off between broadening and observed peak-to-peak height.

The expression for the approximate Lorentzian derivative peak-to-peak height is given by:

$$P_{app} = \frac{\frac{288}{\sqrt{3}} A m T_2 \left[m^2 T_2^2 - 4 + 2\sqrt{m^4 T_2^4 + 4 m^2 T_2^2 + 16} \right]^{\frac{1}{2}}}{8 m^4 T_2^4 + 128 m^2 T_2^2 + 128 + (32 - 8 m^2 T_2^2)\sqrt{m^4 T_2^4 + 4 m^2 T_2^2 + 16}}$$

This expression can be calculated as a function of the product mT_2, which as before, is related to the desired independent variable m/W.

From the experimental spectra in Figures 35 and 36 values of this expression can be abstracted as well.

To correlate these two sets of values for P_{app}, the remaining unknown amplitude parameter, A, is adjusted to force coincidence of the experimental and calculated curves for the smallest values of the independent variable m/W.

These two curves of the calculated and experimental analysis of the effect of the modulation amplitude on the peak-to-peak height are shown in Figure 38.

It would be expected that the experimental curve would be less than the calculated curve. The peak-to-peak height

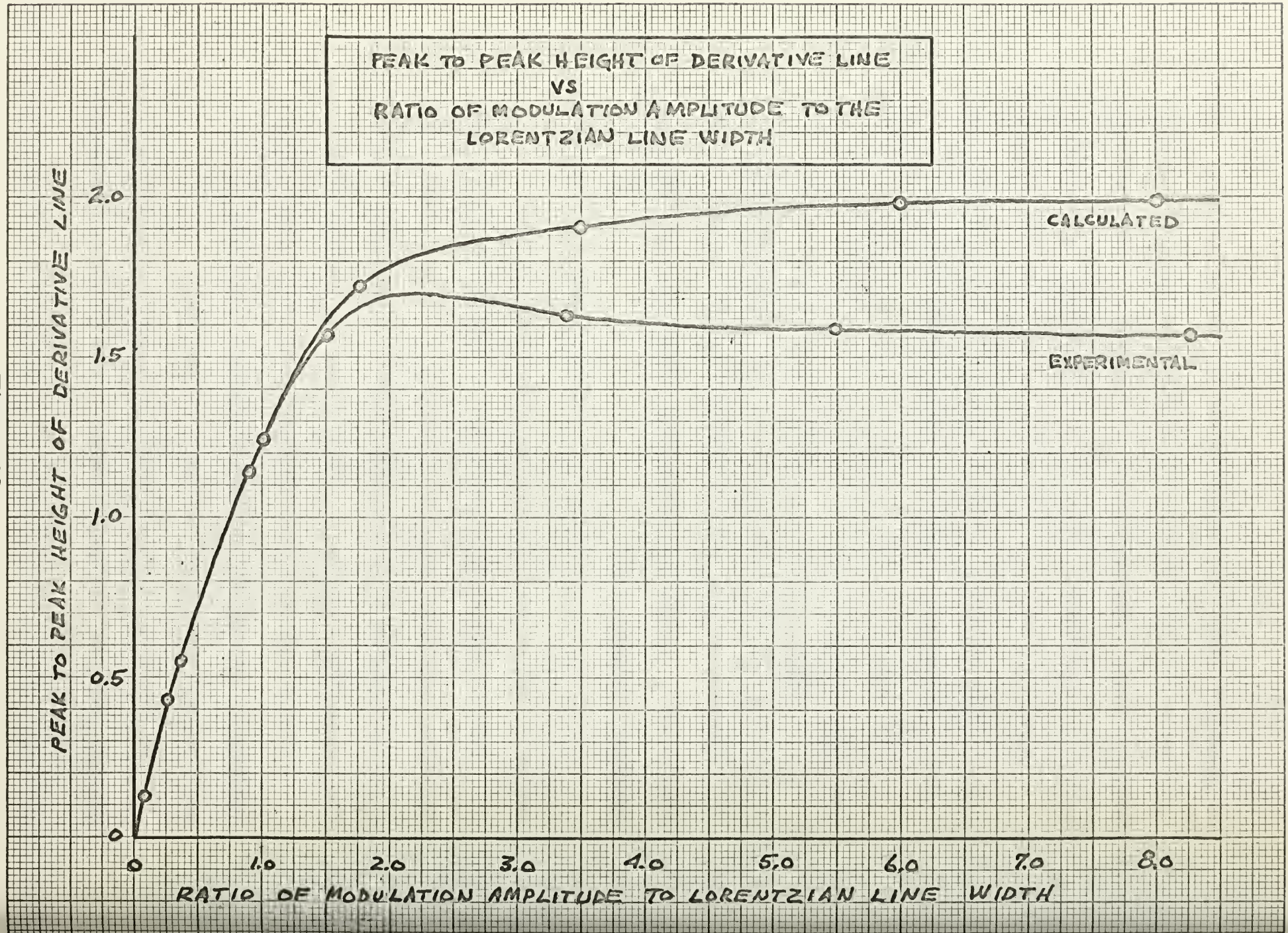

Figure 38

is rather sensitive to losses in responses and attenuations associated with the mechanical and electrical aspects of obtaining a recorded spectrum. For example, an increase in sweep-time from 5 to 10 minutes can increase the observed height by approximately 20% in the cases of narrow line widths. However, beyond a sweep-time of 25 minutes any increase is slight.

The last related aspect of these calculations is that of converting the nominal dial setting of the modulation amplitude on the E.P.R. apparatus into a modulation amplitude in terms of field or other increment of the displayed spectrum.

This conversion can be obtained from the expression for the observed line width.

$$W_{app} = 2\left[\frac{m^2T_2^2 - 4 + 2\sqrt{m^4T_2^4 + 4m^2T_2^2 + 16}}{12T_2^2}\right]^{\frac{1}{2}}$$

Assuming that the observed line width at the smallest value of modulation amplitude is equal to the Lorentzian line width, the line width parameter T_2 can be calculated.

Thus, the above expression reduces to a single unknown m, for each observed line width.

$$m^4T_2^4 + 8m^2T_2^2 + 2T_2^4W_{app}^2m^2 = 3T_2^4W_{app}^4 + 8T_2^2W_{app}^2 - 16$$

This expression can be solved by an iterative technique for a modulation amplitude in Gauss or other display increment corresponding to the dimension of the line width.

This conversion is plotted as the curve in Figure 39 with the modulation amplitude in Gauss as a function of the nominal

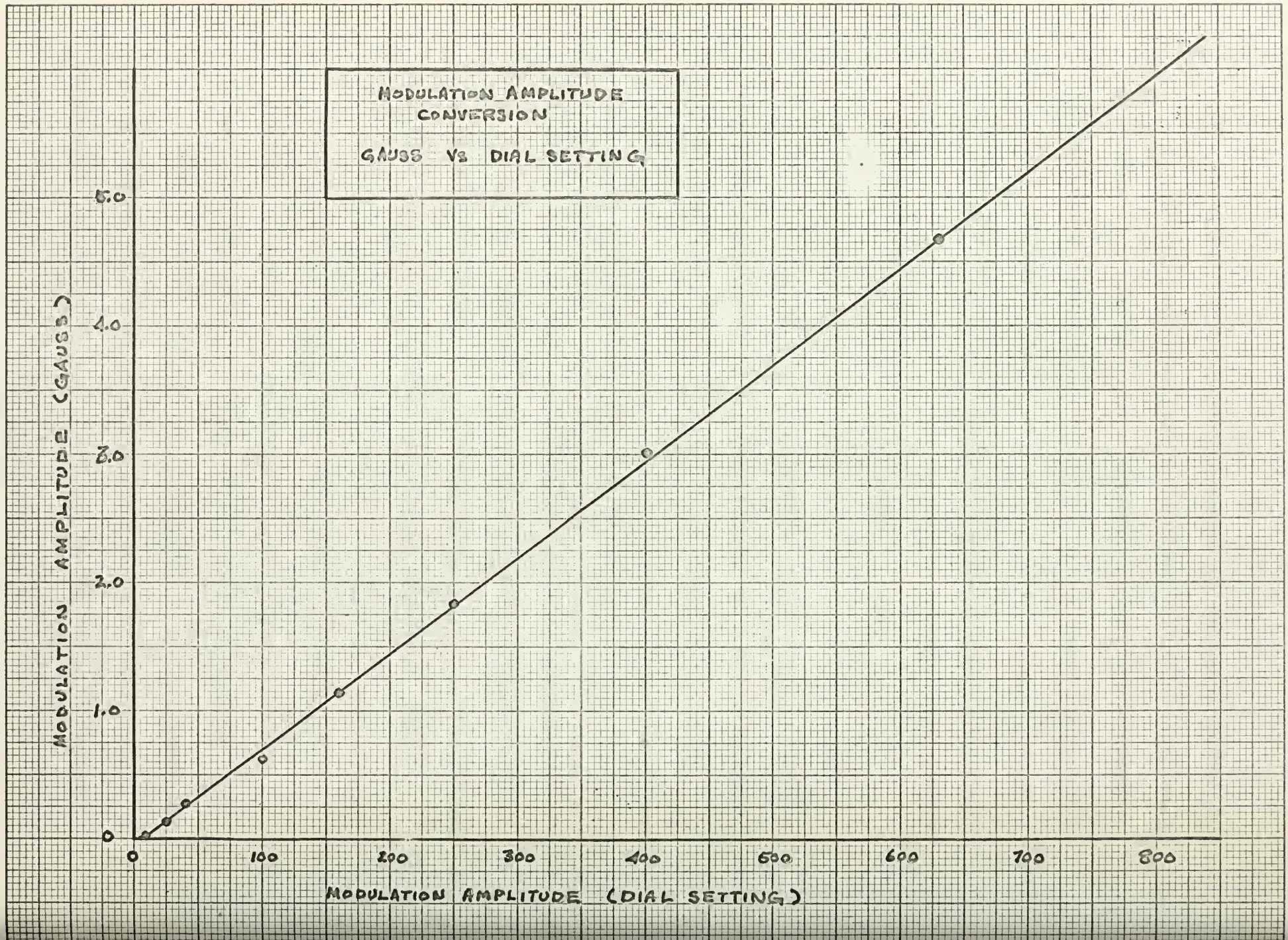

Figure 39

dial setting of modulation amplitude.

Finally, Figures 40 and 41 represent enlarged sections of the previous plots. These represent curves in the area of the largest interest to the experimentalist attempting to avoid modulation broadening.

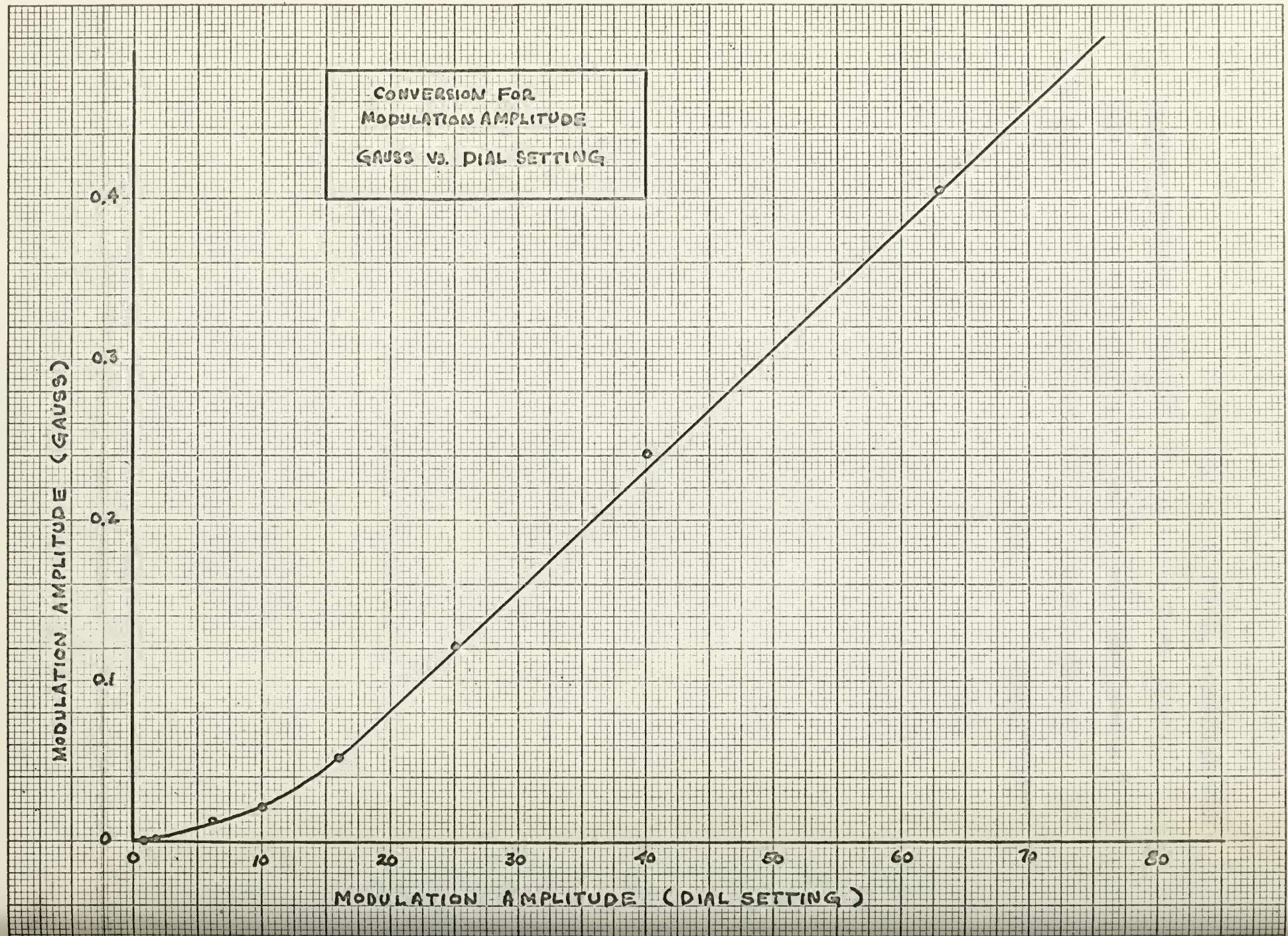

Figure 40

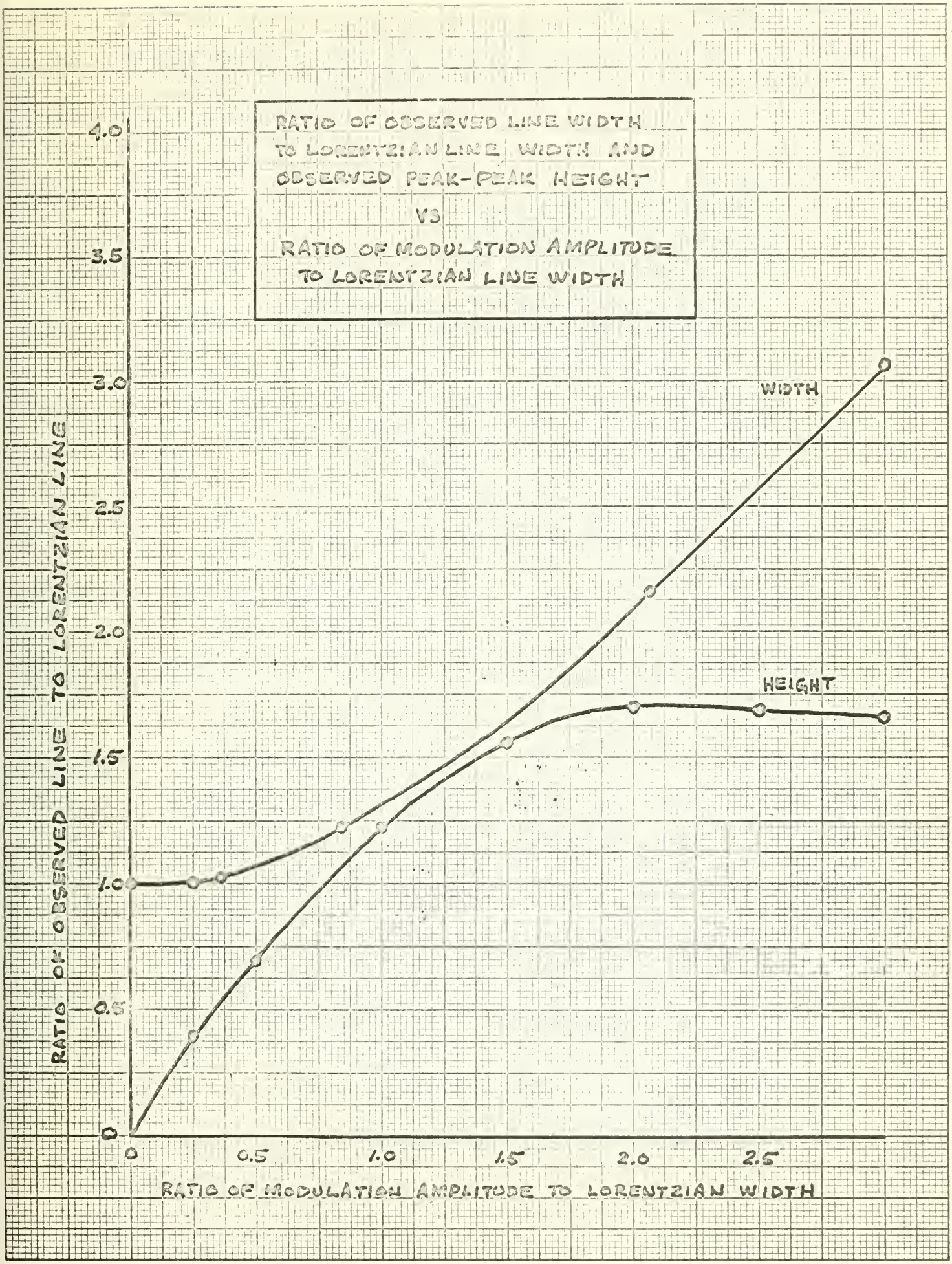
RATIO OF OBSERVED LINE WIDTH TO LORENTZIAN LINE WIDTH AND OBSERVED PEAK-PEAK HEIGHT
VS
RATIO OF MODULATION AMPLITUDE TO LORENTZIAN LINE WIDTH
RATIO OF OBSERVED LINE TO LORENTZIAN LINE
4.0
3.5
3.0
2.5
2.0
1.5
1.0
0.5
0
WIDTH
HEIGHT
0
0.5
1.0
1.5
2.0
2.5
RATIO OF MODULATION AMPLITUDE TO LORENTZIAN WIDTH

Figure 41

INITIAL DISTRIBUTION LIST

		No. Copies
1.	Defense Documentation Center Cameron Station Alexandria, Virginia 22314	20
2.	Library U. S. Naval Postgraduate School Monterey, California 93940	2
3.	Prof W. M. Tolles (Thesis Advisor) Department of Chemistry U. S. Naval Postgraduate School Monterey, California 93940	2
4.	LT Harvey A. Eikel, USN 1075 Lighthouse Avenue, Apt. 215, Pacific Grove, California 93950	1

Security Classification

DOCUMENT CONTROL DATA - R&D

(Security classification of title, body of abstract and indexing annotation must be entered when the overall report is classified)

1. ORIGINATING ACTIVITY (Corporate author)	2a. REPORT SECURITY CLASSIFICATION
U. S. Naval Postgraduate School Monterey, California	UNCLASSIFIED
	2b GROUP

3. REPORT TITLE

ELECTRON PARAMAGNETIC RESONANCE ANALYSIS OF DIMETHYL AMIDOGEN IN POLYCRYSTALLINE TETRAMETHYL TETRAZENE

4. DESCRIPTIVE NOTES (Type of report and inclusive dates)

5. AUTHOR(S) (Last name, first name, initial)

EIKEL, Harvey A., LT, USN

6. REPORT DATE	7a. TOTAL NO. OF PAGES	7b. NO. OF REFS
May 1966	95	45

8a. CONTRACT OR GRANT NO.	9a. ORIGINATOR'S REPORT NUMBER(S)
b. PROJECT NO.	
c.	9b. OTHER REPORT NO(S) (Any other numbers that may be assigned this report)
d.	

10. AVAILABILITY/LIMITATION NOTICES

11. SUPPLEMENTARY NOTES	12. SPONSORING MILITARY ACTIVITY

13. ABSTRACT

The photolytic decomposition of tetramethyl-2-tetrazene yields a short-lived paramagnetic species which is stabilized at liquid nitrogen temperatures. For the analysis of the electron paramagnetic resonance spectrum the species has been identified as the free radical dimethyl amidogen. The hyperfine coupling tensors were assigned on the basis of a polycrystalline line shape analysis. The radical exhibits axial symmetry with the parallel components of the tensors greater than the perpendicular components. The limits of error associated with the components of the tensors were estimated from the general comparison of the calculated and observed spectra. The principal values of the hyperfine coupling and g tensors for the radical are:

A^N isotropic $= 27.9 \pm 3.0$G. $A^N_{\parallel} = 27.9 \pm 3.0$G $A^N_{\perp} = 27.9 \pm 3.0$G.

A^H isotropic $= 26.4 \pm 1.0$G. $A^H_{\parallel} = 28.4 \pm 1.0$G. $A^H_{\perp} = 25.5 \pm 1.0$G.

$g_{\parallel} = 2.0098 \pm 0.0015$ $g_{\perp} = 2.0042 \pm 0.0005$

DD FORM 1 JAN 64 1473

Security Classification

14. KEY WORDS	LINK A		LINK B		LINK C	
	ROLE	WT	ROLE	WT	ROLE	WT
Dimethyl Amidogen Electron Paramagnetic Resonance Polycrystalline Spectrum Analysis Tetramethyl Tetrazene						

INSTRUCTIONS

1. ORIGINATING ACTIVITY: Enter the name and address of the contractor, subcontractor, grantee, Department of Defense activity or other organization *(corporate author)* issuing the report.

2*a*. REPORT SECURITY CLASSIFICATION: Enter the overall security classification of the report. Indicate whether "Restricted Data" is included. Marking is to be in accordance with appropriate security regulations.

2*b*. GROUP: Automatic downgrading is specified in DoD Directive 5200.10 and Armed Forces Industrial Manual. Enter the group number. Also, when applicable, show that optional markings have been used for Group 3 and Group 4 as authorized.

3. REPORT TITLE: Enter the complete report title in all capital letters. Titles in all cases should be unclassified. If a meaningful title cannot be selected without classification, show title classification in all capitals in parenthesis immediately following the title.

4. DESCRIPTIVE NOTES: If appropriate, enter the type of report, e.g., interim, progress, summary, annual, or final. Give the inclusive dates when a specific reporting period is covered.

5. AUTHOR(S): Enter the name(s) of author(s) as shown on or in the report. Enter last name, first name, middle initial. If military, show rank and branch of service. The name of the principal author is an absolute minimum requirement.

6. REPORT DATE: Enter the date of the report as day, month, year; or month, year. If more than one date appears on the report, use date of publication.

7*a*. TOTAL NUMBER OF PAGES: The total page count should follow normal pagination procedures, i.e., enter the number of pages containing information.

7*b*. NUMBER OF REFERENCES: Enter the total number of references cited in the report.

8*a*. CONTRACT OR GRANT NUMBER: If appropriate, enter the applicable number of the contract or grant under which the report was written.

8*b*, 8*c*, & 8*d*. PROJECT NUMBER: Enter the appropriate military department identification, such as project number, subproject number, system numbers, task number, etc.

9*a*. ORIGINATOR'S REPORT NUMBER(S): Enter the official report number by which the document will be identified and controlled by the originating activity. This number must be unique to this report.

9*b*. OTHER REPORT NUMBER(S): If the report has been assigned any other report numbers *(either by the originator or by the sponsor)*, also enter this number(s).

10. AVAILABILITY/LIMITATION NOTICES: Enter any limitations on further dissemination of the report, other than those imposed by security classification, using standard statements such as:

(1) "Qualified requesters may obtain copies of this report from DDC."

(2) "Foreign announcement and dissemination of this report by DDC is not authorized."

(3) "U. S. Government agencies may obtain copies of this report directly from DDC. Other qualified DDC users shall request through _____."

(4) "U. S. military agencies may obtain copies of this report directly from DDC. Other qualified users shall request through _____."

(5) "All distribution of this report is controlled. Qualified DDC users shall request through _____."

If the report has been furnished to the Office of Technical Services, Department of Commerce, for sale to the public, indicate this fact and enter the price, if known.

11. SUPPLEMENTARY NOTES: Use for additional explanatory notes.

12. SPONSORING MILITARY ACTIVITY: Enter the name of the departmental project office or laboratory sponsoring *(paying for)* the research and development. Include address.

13. ABSTRACT: Enter an abstract giving a brief and factual summary of the document indicative of the report, even though it may also appear elsewhere in the body of the technical report. If additional space is required, a continuation sheet shall be attached.

It is highly desirable that the abstract of classified reports be unclassified. Each paragraph of the abstract shall end with an indication of the military security classification of the information in the paragraph, represented as *(TS)*, *(S)*, *(C)*, or *(U)*.

There is no limitation on the length of the abstract. However, the suggested length is from 150 to 225 words.

14. KEY WORDS: Key words are technically meaningful terms or short phrases that characterize a report and may be used as index entries for cataloging the report. Key words must be selected so that no security classification is required. Identifiers, such as equipment model designation, trade name, military project code name, geographic location, may be used as key words but will be followed by an indication of technical context. The assignment of links, roles, and weights is optional.